Performance of a Population of Independent Filaments in Lamellipodial Protrusion

Thomas E. Schaus* and Gary G. Borisy*†
*Department of Cell and Molecular Biology, Northwestern University Feinberg School of Medicine, Chicago, Illinois; and †Marine Biological Laboratory, Woods Hole, Massachusetts

ABSTRACT Actin polymerization is responsible for moving a wide variety of loads, from the protrusion of membrane-bound filopodia and lamellipodia of immune, cancer, and other motile cells, to the propulsion of some intracellular pathogens. A universal explanation of the forces and velocities generated by these systems has been hampered by a lack of understanding in how a population of independent filaments pushes these loads. Protrusion of a lamellipodium by the very filaments supporting the membrane load is thought to operate by the Brownian ratchet mechanism, with overall organization governed by the dendritic-nucleation/array-treadmilling model. We have incorporated these two models into a two-dimensional, stochastic computer model of lamellipodial protrusion, and studied how force and velocity generation varied under different assumptions. Performance is very sensitive to the extent to which the work of protrusion is shared among individual polymerization events within the filament population. Three identified mechanisms promote this "work-sharing": 1), Most systems, including lamellipodia, utilize a self-organizing distribution of filament-load distances which serves to decrease the effective size of a monomer and dramatically improve performance. 2), A flexible membrane allows for consistent performance over wide leading edges. 3), Finally, very flexible filaments are capable of sharing work very uniformly, and therefore, of near-perfect theoretical performance. Transient tethering to the lamellipodial membrane limits their efficacy, however, and mandates a minimum filament stiffness. Overall, we estimate lamellipodia to operate with 40-nm bending-length filaments and low characteristic tether forces. Modeled lamellipodia exhibit sigmoidal force-velocity relationships and share the work of protrusion only moderately well among filaments, performing at approximately one-half of theoretical force and velocity maximums. At this level of work-sharing, the natural monomer size is optimal for generating velocity.

INTRODUCTION

Actin-based motility is ubiquitous in health and disease processes. Developing neurons, metastatic cancer cells, and infection-fighting white blood cells extend actin-driven lamellipodia and filopodia in whole-cell motility (1). Likewise, enteric pathogens such as *Listeria monocytogenes* and *Shigella flexneri* direct the cell's actin machinery to propel them into adjacent cells (2). Various biophysical models of protrusion have been contemplated (3–9), but the exact mechanisms of force generation on a molecular level are still being debated.

It was initially predicted by thermodynamic arguments that the free energy of actin polymerization itself can perform useful work against a load (10,11). That is, neither molecular motors nor any type of nucleotide hydrolysis is strictly necessary. Several experiments subsequently validated this. For example, the encapsulation and subsequent polymerization of actin monomers within a liposome was shown to change liposome morphology from spherical to rigid dumbbell or disk-shaped (12). Later, *Listeria*-like movement propelled by actin comet-tails was reconstituted with both pathogens and synthetic beads in motor-free, purified protein systems (13,14). More recently, polymerizing actin filaments have been made to exert forces on experimental cantilevers and optically trapped beads (15,16).

It is the fast-growing barbed-ends of working actin filaments that support the membrane or pathogen load, and the paradox that actin monomers must intercalate between the filaments and the load they bear has been apparent for some time. Peskin et al. proposed a Brownian-ratchet mechanism to explain this propulsion, wherein transient gaps between rigid filaments and their load were created by Brownian motion (thermal fluctuations) of the load and rectified by polymerization (9). While this analysis applied to various geometries, including those with flexible membranes, then-undiscovered filament-load tethering prevented many experiments from showing the expected dependence of velocity on bacterial size (2,17). The Brownian-ratchet mechanism was subsequently modified by Mogilner and Oster under the assumption that it is not the load itself that diffuses, but the filaments that bend under thermal motion to create gaps (7). In both of these models, the authors solved a Fokker-Planck equation governing the discrete polymerization of filaments in a gap created by Brownian motion; the differences involved the calculation of the probability of a gap. Under the assumption that thermal fluctuations are much faster than the polymerization rates, Peskin et al. concluded that free polymerization rates are simply reduced by a Boltzmann factor ($e^{-\Delta E/kT}$) to account for the probability that a sufficient gap

Submitted November 1, 2007, and accepted for publication March 20, 2008.
Address reprint requests to Thomas E. Schaus, E-mail: tschaus@northwestern.edu.
Editor: Alexander Mogilner.

0006-3495/08/08/1393/19 $2.00
doi: 10.1529/biophysj.107.125005

exists. When the work of protrusion was significant compared to the thermal energy available, Mogilner and Oster came to the same conclusion with filament bending. In either case, the gap required the concentration of at least ΔE of thermal energy into a mechanical potential energy sufficient to separate the filament and load. In fact, both filament and load fluctuations are thought to contribute to real ratchet motility, depending on the particular system.

Both Brownian-ratchet models estimated the behavior of a population of pushing filaments by calculating the behavior of a single filament under the average load. Because polymerization is a distinct and rapid kinetic event compared to the time interval between serial events of a population, however, a single polymerization event may perform much more work on the load than the average event. Such a high-energy (low probability) event would be followed by other, low-energy polymerization events effectively subsidized by the lead filament (7). (This is similar to the case of microtubule dimers (18)). This uneven distribution of work among events likely diminishes overall system performance, but it was difficult for the published analytical models to take these variations into account. Stochastic, numerical models incorporating many individual filaments can build upon those more fundamental results by allowing for a geometric complexity not achievable analytically. Such models of populations of polymerizing filaments have been developed (3,4,19), but have not been used in a detailed analysis of mechanisms of lamellipodial protrusion, nor were generally capable of modeling flexibility in both plasma membranes and filaments. Atilgan et al. appeared closest, analyzing filopodial protrusion with flexible membranes but rigid filaments, but they made no attempt to model lamellipodia or the transient tethering of filaments to the membrane (20). Furthermore, experiments continue to generate sometimes conflicting data on protrusive rates and force-velocity relationships for a variety of geometries (15,16, 21–23). A more complete analysis of this energetically complex system is critical to the prediction—and interpretation—of the velocities and forces that a population of filaments can generate.

We have developed a stochastic, two-dimensional computer model of lamellipodia, encompassing filament and associated kinetic reactions, monomer diffusion, and filament and plasma membrane flexibility (24). The model takes into account the interaction between each filament and a rigid or flexible leading edge (LE) individually, calculating the required energies and probabilities of each polymerization event separately. This model is presented here as an extension of the previous analytical efforts to model protrusion velocities against an average load, and relies on their analysis of the applicability of the simplified Boltzmann result to this system. It indicates the instantaneous, local protrusive rate, and does not address higher-level behaviors such as whole-cell motility or retrograde flow. We first analyze ideal assumptions regarding the perfect sharing of propulsive work among polymerization events, compare the performance of this perfect system to that of a system with zero work-sharing, and designate an envelope (i.e., limits, or ranges, of performance) within which real systems must operate. We then show the extent to which protrusion rate and force generation are improved by three putative mechanisms of work-sharing, enabled by the distances between filament ends and load, plasma membrane flexibility, and filament flexibility. These mechanisms serve to improve performance within the theoretical limits. Taking a narrow section of lamellipodium as a base case, different combinations of mechanisms are considered separately to demonstrate their relative effects and to contrast results to more rigid systems such as beads/pathogens and filopodia. Finally, we consider the transient tethering of branched filaments to the membrane of lamellipodia and estimate overall lamellipodial performance.

THEORETICAL MODEL OF PERFORMANCE LIMITS

In traveling through connective or other tissue to reach a destination, cells must generate sufficient protrusion velocities and forces. This suggests the use of protrusion rate, V_p, and stall force as metrics of protrusion effectiveness. The true thermodynamic stall force, $F_{stall} = F_0$, at which V_p is exactly zero, does not vary with the precise mechanism of protrusion. Its value is simply $N_{fb}/(\delta \cos\phi)\ \ln(k_{on}[A]/k_{off})$, where N_{fb} is the number of pushing (free) barbed ends; $(\delta \cos\phi)$ is the distance a tip at angle ϕ grows, upon polymerization, in the direction of protrusion; k_{on} and k_{off} are the kinetic polymerization rate constants; and $[A]$ is the local concentration of competent actin monomers (see Table 1 for symbol definitions). As we will show, however, protrusion of many systems falls to insignificant rates at load forces far below the true stall force. We therefore report an effective stall force, $F_{0.5}$, at which protrusion rates are decreased to 0.5 μm/min ($\approx$2.5% of the free elongation rate for the Table 2 values used in this report). The metrics of V_p and $F_{0.5}$ represent values which are both significant to the cell and measurable in simulation or wet lab experiment.

Theoretical estimates of V_p and $F_{0.5}$ exist. In protrusion, polymerizing lamellipodial actin filaments perform work on the plasma membrane against a combination of internal (membrane and tethering) and external (adjacent tissue) load forces. Given a total amount of work done on the leading edge in protruding it a large distance, a varying amount of work is potentially done with each of many isolated polymerization events. The extent to which the total work is distributed evenly among polymerization events is termed the level of ''work sharing'' in this article, and we will show that it has a strong effect on the abovementioned metrics of performance. The word ''work'' was chosen over the word ''load'' because, traditionally in mechanics, ''work'' refers to energy changes (i.e., force $\times$ distance) while ''load'' merely refers to forces. As such, we are not referring to a sharing of ''load'' but of ''work,'' a value equal to the change

TABLE 1 Symbols

V_p; V_{free}	Velocity of the LE center of mass; free polymerization velocity.
ΔE	Thermal energy required for intercalating a monomer between LE and barbed end over successive potential states.
ϕ	Filament orientation angle, with respect to the direction of protrusion.
$[A]$; $[A]_{i,j}$	ATP-G-actin concentration, in general; local concentration at position (i,j).
F_T	Force between membrane and tethered filament, transmitted through the arp2/3-activator tether.
R_{dT}	Force-dependent rate of detethering reaction between arp2/3 and membrane-bound activator.
$\dot{W}$	Total rate of work in pushing load F, performed by all filaments N_{fb}.
$\dot{n}$	Total polymerization rate (monomers per time for all filaments N_{fb}).
ΔE_{avg}	Average thermal energy required to create a gap for a polymerization event.
ΔE_i	Thermal energy required for event i.
$F_{0.5}$	Total (membrane and external) load force density at which protrusion is reduced to 0.5 μm/min.

in the potential energy ΔE of the system. This is the value that governs individual reaction rates.

Neglecting tethering between branched filaments and the membrane, Appendix A shows that the average work performed by each event is always $\Delta E_{avg} = (F_L \delta \cos\phi)/N_{fb}$, where F_L/N_{fb} is the average load force per pushing filament. If every individual polymerization event performs this average amount of work, the resulting relationship between protrusion rate and total load force F_L is the familiar

$$V_P = (\delta \cos\phi)\left[k_{on}[A]\, e^{\frac{-F_L \delta \cos\phi}{N_{fb} kT}} - k_{off}\right]. \quad (1)$$

Equation 1 assumes that only the kinetic on-rate is affected by the load, though thermodynamic analysis concludes only that the ratio of effective k_{on}/k_{off} decreases by the Boltzmann factor. While the distribution of the effect of load on the on- and off-rates is unknown, most authors intuit and assume that the effect is primarily to reduce the polymerization reaction. We do the same and assume a constant off-rate.

Appendix B further shows that Eq. 1 represents the best performance the system can theoretically attain, and any deviation from the perfect sharing of work among polymerization events results in both slower protrusion rates and lower effective stall forces. Fig. 1 *a* plots this perfect work-sharing (PWS) relationship in the form of the force-velocity curve sometimes generated in experiment. Fig. 1, *b* and *c*, plot the protrusion rate V_p and effective stall force $F_{0.5}$ as a function of the number of free (pushing) barbed ends, N_{fb}, where the value of $F_{0.5}$ is the force F_L in Eq. 1 at which $V_p = 0.5$ μm/min. The curves are plotted using parameters in Table 2 and for the equivalent of a 150-nm-wide section of lamellipodia: 30 filaments in Fig. 1 *a* and a 15-pN load in Fig. 1 *b*.

Perfect work-sharing represents the thermodynamic upper limit of performance, but not necessarily the performance

TABLE 2 Model parameters and standard values

Symbol	Value	Description	References
δ	2.7 nm	Extension length of polymerizing actin monomer.	—
D	6.0 $\mu m^2/s$	Cytoplasmic actin monomer diffusion coefficient.	(28)
$[A]_{TE}$	12 μM	Fixed, trailing-edge actin monomer concentration.	(29)
γ_{se}	50 pN/nm	Plasma membrane surface energy coefficient (= 50 pJ/nm^2).	(8,30)
F_L	100 pN/μm	Total load force (linear density) against LE protrusion (= 2 γ_{se} for internal membrane forces alone, because lamellipodia contain two membrane surfaces). Higher values represent additional external loads.	—
f_L	15 pN	Total membrane (nontethering) load force against protrusion = $F_L \Delta x$.	—
Δx	150 nm	Standard width of lamellipodial LE modeled (governs n_{fb} and f_L).	—
κ_b	80 pN nm	Bending energy coefficient, ~20 *kT*.	(30)
L_p	10 μm	Persistence length of actin filaments.	(31)
t_{lam}	200 nm	Lamellipodial thickness.	(29)
$k_{on,brb}$	12/μM/s	On-rate of actin to barbed end $\equiv R_{pol,b}/[A]$.	(32)
$k_{off,brb}$	1.4/s	Off-rate of actin from barbed end $\equiv R_{dpol,b}$.	(32)
$k_{on,ptd}$	0/μM/s	On-rate of actin to pointed end, profilin-adjusted $\equiv R_{pol,p}/[A]$.	(33)
$k_{off,ptd}$	8.0/s	Off-rate of actin from pointed end, cofilin-adjusted $\equiv R_{dpol,p}$.	(34)
ε	1.5 δ	LE cap-protection/branch zone (Y) length.	(3,24)
R_{br}	0.43/s	(Total) rate of barbed end branching $\equiv k_{br}$ [*arp2/3*].	(8,24,29)
R_{dbr}	0.05/s	Rate of debranching for any branch point.	(35)
$k_{off,T}$	0.5/s	Unloaded (natural) off-rate of arp2/3 activator to arp2/3.	(8)
$F_{char,T}$	2 pN	Characteristic force describing force-dependence of branch tether.	See text
R_{cp}	6.0/s	Rate of barbed end capping $\equiv k_{on,cp}$ [*cp*].	(36)
R_{uncp}	0/s	Uncapping rate for any capped barbed end $\equiv k_{off,cp}$.	(36,37)
N_{fb}	200 fil/μm	Forward-facing free barbed ends per LE width (indirectly specified).	(29)
n_{fb}	30 fil	Number of filaments in a 150-nm-wide LE, corresponding to N_{fb}.	—
θ_{br}	70°	Average branch angle.	(38)
σ_{br}	7°	Branch angle standard deviation.	(38)

See model description and mathematical relationships in Schaus et al. (24).

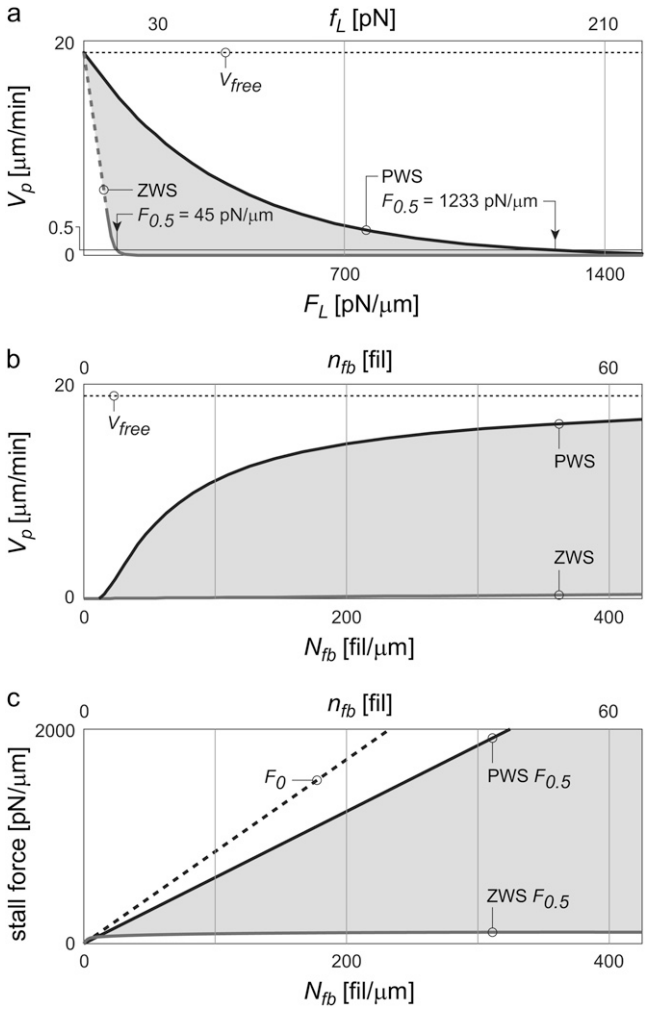

FIGURE 1 Theoretical values of protrusion rate and force generation vary widely, depending on how evenly the work of protrusion is shared among filaments. Real systems (without branch-tethering) are expected to operate somewhere within the shaded ranges shown. (*a*) Plotted as force-velocity curves, velocities of zero and perfect work-sharing systems (ZWS and PWS, respectively) vary widely. The effective stall forces ($F_{0.5}$) are noted. (*b* and *c*) The ranges for protrusion rate (V_p) and $F_{0.5}$ are also wide as a function of the number of pushing barbed ends (N_{fb}). Curves represent manipulations of Eqs. 1 (PWS) and 2 (ZWS) plotted for 30 filaments (in panel *a*) or acting on a 15 pN load (in panel *b*), the equivalent of a 150-nm-wide section of lamellipodial LE.

attained by any real mechanism of protrusion. In light of the discrete, stochastic nature of polymerization, wherein individual filaments add a fixed length in random order, actual protrusion likely entails some variation in protrusive work among polymerization events. This variation can be a result of varied opposing force and/or protrusion distance. The worst-case performance is returned by a system with the widest possible distribution of work: a lead polymerization event does the maximum possible protrusion work, $\Delta E_{max} = (F_L \delta \cos\phi)$, and all other filaments subsequently add a monomer without impinging on the load at all, performing zero work each (Appendix C). This results in the same average ΔE_{avg}, but a much lower protrusion rate:

$$V_P = N_{fb}(\delta \cos\phi)\, k_{on}[A]\, e^{\frac{-F_L \delta \cos\phi}{kT}}. \quad (2)$$

Equation 2 represents zero work-sharing (ZWS), and provides the lower bound of possible velocities in Fig. 1, *a* and *b*. It neglects the kinetic off-rate, which makes little absolute difference, and is only valid at low V_p/V_{free}. The effective stall force, $F_{0.5}$, is plotted in Fig. 1 *c*. The limits of performance in Fig. 1, *a–c*, represent the wide ranges somewhere within which real systems must operate. The extent to which a system shares the work of protrusion among polymerization events governs its performance within these limits.

Three mechanisms allow a population of Brownian ratchets to share the work of protrusion among polymerization events. The ZWS condition, in which the barbed ends of all rigid filaments begin at zero distance from the rigid LE and at the same orientation angle, is diagrammed in Fig. 2 *a*. It is evident that the lead polymerization event performs all of the work. A similarly rigid system which is instead initialized at a distribution of distances from the LE (Fig. 2 *b*) allows the most-recently polymerized filament to support the LE, and working filaments to polymerize from farther back and advance the LE a fraction of one monomer length. This *fractional* protrusion results in a distribution of required energies between that of PWS and ZWS, and can therefore be expected to lead to faster and more forceful protrusion. The addition of a flexible LE (i.e., a plasma membrane) in Fig. 2 *c* allows for *local* extension of the LE, limiting the maximum energy burden by distributing the work of polymerization among filaments spatially. Finally, flexibility in the filaments themselves allows for *simultaneous* work by multiple filaments (Fig. 2 *d*). An LE-resisting protrusion compresses (bends) multiple filaments at once, spreading the load forces among them. Upon polymerization, both the newly lengthened filaments and the other compressed filaments share the work of protrusion as they straighten. All three of these mechanisms, fractional (via distance distribution), local (via membrane flexibility), and simultaneous protrusion (via filament flexibility), may increase the protrusion rate and effective stall force by more evenly sharing the total work of extension among individual polymerization events.

One, two, or all three mechanisms may operate in the same system, depending on geometry. Almost any real system would seem to allow for filaments to vary in tip distance from the load. Rigid systems such as parallel filament bundles pushing against experimental cantilevers or beads (15) might require a variation in the position of filament nucleation to enable this effect. More flexible systems would certainly allow for this variation in geometry (filament orientation, position, and flexibility). Intracellular pathogens and beads, with filaments nucleated by arp2/3 at a large angle to the load, might allow for fractional and simultaneous work-sharing by way of filament flexibility (13,16,21,22), while filopodia

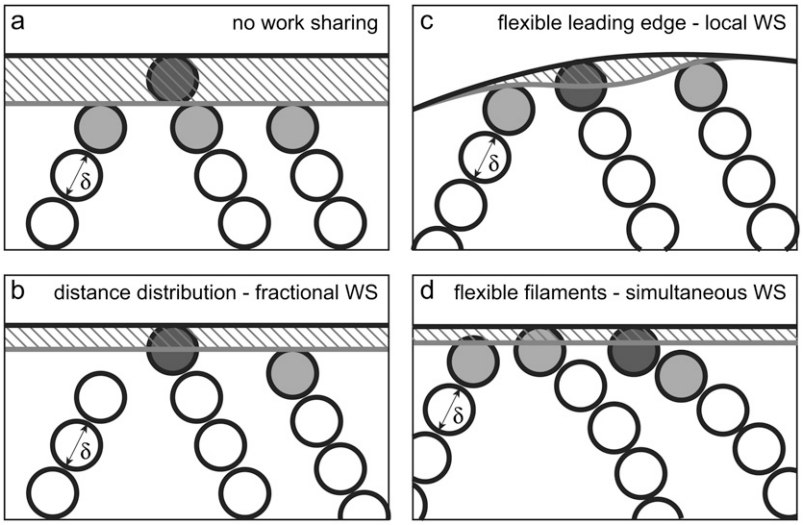

FIGURE 2 Three mechanisms allow for the sharing of work more evenly among polymerization events, thereby increasing protrusion rate and effective stall force. In each diagram, a gray LE initially supported by gray filament tips is advanced by polymerization of a solid monomer. (*a*) A rigid system in which filaments are integer numbers of monomer from the LE exhibits zero work-sharing, with events performing either maximal (solid monomer) or zero work (others catching up). (*b*) Randomization of filament-LE distances allows for polymerization events to effectively push the LE a fraction of a monomer forward. (*c*) Flexibility in the load allows events to protrude the LE only locally. (*d*) Finally, multiple flexible filaments exert protrusive forces on a load simultaneously and reduce the load force per filament. In each case, the amount of work performed is roughly proportional to the hatched area.

might allow for fractional and local work-sharing by way of a flexible load (20). Lamellipodia and analogs likely use all three mechanisms of work-sharing together to improve performance (23,25,26). The relative contributions of these mechanisms and the total extent of work-sharing are not known.

NUMERICAL MODEL OF PROTRUSION

The model is a hybrid of spatially discretized diffusion of soluble actin monomers, Monte Carlo (stochastic) filament kinetics, and iterative calculations of flexible membrane and filament mechanics (Fig. 3). A constant-thickness rectangular region was modeled, bounded by the leading edge (LE), cyclic boundaries on the lateral sides, and a filament-absorbing trailing edge. Every filament throughout the thickness t_{lam} was modeled, keeping track of the X and Y positions (perpendicular and parallel to protrusion, respectively) and states of each end, but values were not resolved in the Z direction and steric hindrance between filaments was ignored. Diffusion between rectangular areas of an ≈100 nm grid was calculated with a discretized Fick's relationship, with con-

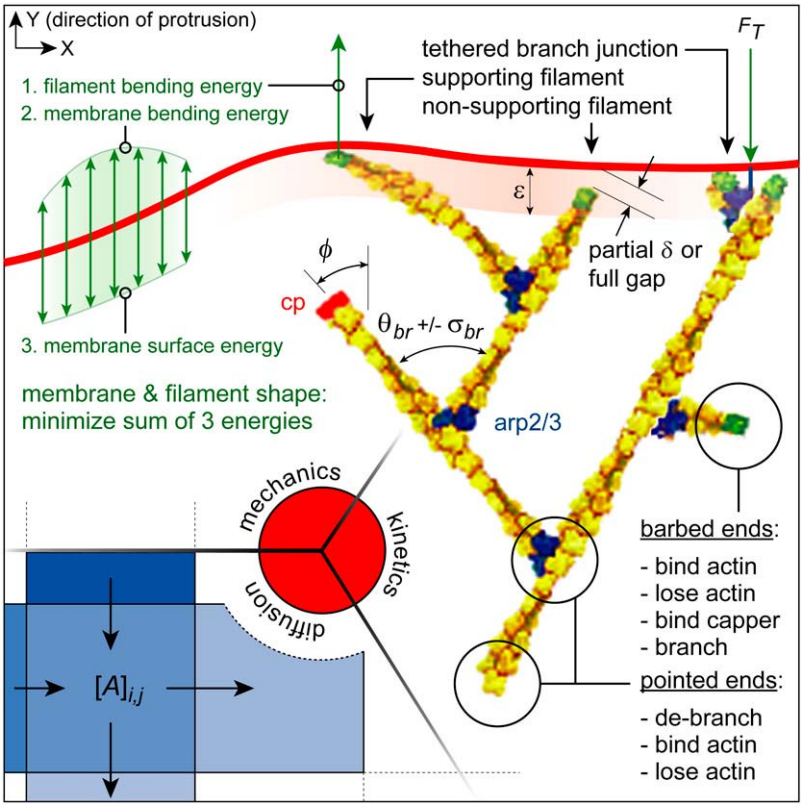

FIGURE 3 The two-dimensional lamellipodial computer model is comprised of three submodels: i), A discretized diffusion model redistributes soluble monomers among rectangular areas of a two-dimensional grid. ii), A kinetics model accounts for all filaments individually and the main kinetic reactions of each. Kinetic polymerization rates and branch junction detethering rates are adjusted for each event, accounting for individual energetics and forces. iii), Mechanical models of the plasma membrane and filaments enable calculation of overall geometry and the aforementioned energetics of polymerization.

centrations assumed uniform within each discretization rectangle and held fixed at the trailing edge. Actin polymerization reactions occurred at a rate proportional to the local actin monomer concentration, and both polymerization and depolymerization reactions were accompanied by monomer exchange with the local soluble pool. In addition to these kinetic reactions, branching, debranching, and capping were modeled. Over each (small) time-step, a Monte Carlo algorithm applied the probability of each reaction. Free barbed ends with tip positions within a *Y*-distance ε from the LE, branched new filaments at a constant rate and were protected from capping. Branching reactions were accompanied by temporary tethers between nascent filament and membrane, with detethering rates (R_{dT}) dependent on the tensile force (F_T) applied as follows: $R_{dT} = k_{off,T}\, e^{F_T/F_{char,T}}$ (8). The branching reactions occurred in the plane of simulation, about the average branch angle ($\theta_{br} \pm \sigma_{br}$), and the branch rate R_{br} was adjusted to result in the specified filament density N_{fb} unless otherwise stated. Capping reactions were considered permanent.

When polymerization resulted in protrusion, the free kinetic on-rate was reduced by a Boltzmann factor ($e^{-\Delta E/kT}$) to account for the probability that the required thermal energy (ΔE) was available to create at least a monomer-size space between the filament and LE. The off-rate remained constant. Beginning and end-states of system geometry (i.e., equilibrium states) were computed by minimizing the total mechanical potential energy, with the potential energies of flexible filament and membrane components described analytically. The difference between potential energies of these kinetic states was used in the Boltzmann factor, and no regard was paid to the mechanical path taken between states. Because thermal fluctuations of the system occurred on a much shorter timescale than the time between monomer additions, each (de)polymerization event was treated independently.

Both filaments and the LE could be modeled as flexible or rigid. A straight, rigid LE was maintained perpendicular to the direction of protrusion and under a constant total resistive force ($f_L = F_L \Delta x$). A two-dimensional, flexible membrane model behaved in a bending-resistant manner and opposed protrusion locally via a surface energy term ($F_L = 2\gamma_{se}$). For the purposes of computation, this flexible LE was divided into ≈30-nm Bezier segments, the nodes of which were adjusted iteratively until the potential energy of the system was minimized. All filaments had pointed ends (free or branched) fixed with respect to the substrate. Rigid filaments also had fixed barbed-end positions and represented immovable points supporting the LE. Flexible filaments were modeled with cantilever beam-bending relationships, allowing their barbed ends to be displaced under load. Model symbols are described in Table 1, and ''standard'' model parameters enumerated in Table 2 were used unless otherwise noted. See Schaus et al. (24) for a complete description of the model and mathematical relationships, and that article's Supplementary Material for an online movie highlighting the details of protrusion.

RESULTS AND DISCUSSION

In a rigid system, filament barbed ends self-organize in distance from the load and exhibit fractional work-sharing

Filaments cannot do work against a load using the Brownian ratchet unless a gap is somehow created by thermal motion. In a relatively rigid system, where filament and LE (load) flexibility contribute little to creating the gap, Peskin et al. (9) showed that rapid diffusion of the entire load allows for the accurate application of the simple Boltzmann factor described above. Here we assume that these conditions are met.

The rigid system considered here is intended as a basis for comparison to other modes of work-sharing. Real examples of a rigid system include parallel bundles of filaments pushing experimental cantilevers or optically trapped beads, sometimes used to measure actin force-velocity relationships (15). The rigid description also applies to systems with filaments at oblique angles to the load, such as in branching systems, provided filament length is kept very short (rigid) by rapid branching and cross-linking, and the number of filaments remains constant. We chose the equivalent of a $\Delta x =$ 150-nm wide section of lamellipodium to model, corresponding to an $f_L = 15$ pN rigid load resisting 30 filaments growing at $\phi = \pm 35°$. Note that this width is important when considering a rigid LE, as scaling the load and number of filaments does not result in the same performance. The resulting average protrusion rate V_p was 6.7 μm/min, or 0.35 V_{free}.

In a polymerization event, the work performed on the load depends in part on how far the load is moved, and so in turn on the initial position of the barbed end. It is a product of the total load force, f_L, and the distance the LE is actually protruded, (δ-d) cosϕ. The maximum work a polymerization event can perform in this system is thus $\Delta E_{max} =$ (15 pN)(2.7 nm)(cos 35°)/(4.1 pN nm/kT) = 8.1 kT for a full monomer at 35°, yielding a low relative extension probability of $e^{-8.1} =$ 0.0003. This work decreases to zero linearly with increasing prepolymerization tip-load distance d, though the probability of extension changes exponentially (Fig. 4 *a*). Even if a filament polymerizes from a distance 0.7 δ from the LE, causing a 0.3 δ protrusion, it still does so at a low relative rate of $e^{-(0.3)(8.1)} = 0.09$. From a uniform initial distribution of barbed-end distances over 1 δ, these effects caused the 30-filament system to self-organize in distance from the load (Fig. 4 *b*), peaking in number at ≈0.65 δ. (The relatively high fraction at distance zero reflects the condition that there is always one filament supporting the load, while the other filaments are distributed among small bins in data acquisition. In this case, 1/30th of the filaments is always touching the LE.) These filaments did work at the rate indicated, with the

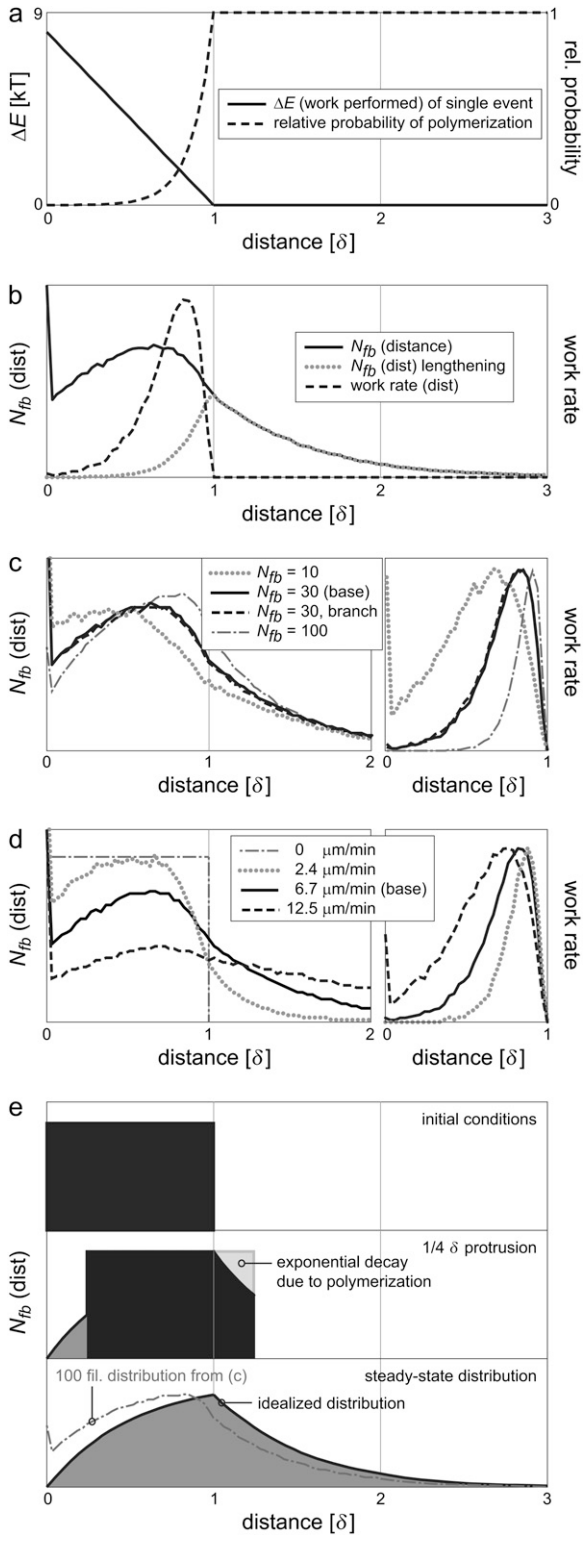

FIGURE 4 Fractional work-sharing emerges naturally in rigid systems. (*a*) The work performed on the LE increases linearly with (prepolymerization) proximity to the LE, causing the probability of polymerization to decrease exponentially. (*b*) A natural distribution of barbed end distances develops, with recently polymerized filaments supporting the load and impeded filaments performing subsequent work. This phenomenon is not affected by (*c*) load force or branching (all at a constant 6.7 μm/min), nor (*d*) by the speed itself (all at a constant 30 filaments). (*e*) A simplified model explains the development of the general distribution shape (see text).

peak work rate performed by filaments $\approx$0.85 δ from the load. The distributions of Fig. 4 *b* contrast sharply with those of a system in which filaments are positioned in-register, with only distances of integer numbers of monomers possible (i.e., at distances 0, δ, 2 δ...). That system would exhibit zero work-sharing, with all work performed from, and all ends typically positioned at, the LE.

These patterns of filament distance and work are general outcomes over a wide range of load forces, filament orientation angles, and branching and capping behaviors. Considering protrusion at the same rate of 0.35 V_{free}, Fig. 4 *c* (*left*) plots distance distributions of barbed-end count for high and low loads. At high load (29.1 pN), 100 filaments are required for the same protrusion rate, and the peak of the distribution is shifted backward to 0.83 δ. At low load (8.1 pN), 10 filaments peak in position somewhat ahead of the base case, at 0.45 δ. A condition in which 30 filaments continuously branch (no tethering, $\varepsilon = 2\ \delta$) at 70° exhibit a very similar distribution to that of the base case. (The spatial profile of the ε-demarcated branching zone is immaterial, since a single filament traverses the zone many times between each branching or capping event.) All of these comparison cases have work largely performed by impeded filaments (shown in Fig. 4 *c*, *right*). Systems with filaments oriented perpendicular to the LE, as well as those with random (forward) orientations, display similar position and work distributions (not shown). We conclude that, at significant loads, neither filament orientation, nor total load, nor branching or capping, disrupts the characteristic distribution of working filaments.

Maintaining a consistent number of growing filaments, we then varied the load force to cause a variation in protrusion rate. Initial conditions of uniform distribution over 1 δ were identical to the conditions found if the system is later stalled (Fig. 4 *d*, *left*). If allowed to travel at low rates of 0.13 V_{free}, the characteristic shape just begins to form. At high protrusion rates of 0.65 V_{free}, the distribution maintains the peak location but appears stretched out over a larger distance from the LE. Again, each of these systems generates the bulk of protrusive work by polymerizing from an impeded position (Fig. 4 *d*, *right*).

The shape of the characteristic barbed-end distribution can be explained with the diagram of Fig. 4 *e*. Let us make a temporary simplifying assumption that the load is not driven by the filaments themselves but moves at a fixed velocity, such that filaments closer than 1 δ from the LE cannot polymerize. From an initially uniform distribution of positions (rectangle), the system is activated and protrusion begins. From the perspective of the LE, the filaments move retrograde, to the right. As filaments increase in distance from the LE, those moving beyond 1 δ find themselves suddenly free to polymerize at a constant rate in time (the free rate), and

thus their count decays exponentially in time and distance. Polymerizing filaments move exactly 1 δ forward in position, creating the congruent shape near the LE and eventually the steady-state distribution shown. This model compares well with the distributions measured, most closely to that of the high-load, 100-filament case. The difference is due to the fact that filaments just ahead of 1 δ, while polymerizing at a reduced rate, are in fact the cause of protrusion. The peak in the modeled distribution thus reflects the early polymerization events that begin the decay before reaching 1 δ. This distribution is both an effect of, and strengthens, the fractional work-sharing of the population. These experiments demonstrate that rigid systems self-organize in position, such that recently polymerized filaments support the LE, while other filaments work to protrude the load in low-energy, fractional steps of $< \delta$.

Fractional work-sharing is an effective mechanism of generating protrusion velocity

We sought to quantify the performance of fractional work-sharing, with respect to the limits of PWS and ZWS, by analyzing the distribution of work among filaments and the resulting protrusion rate and effective stall force. The same base case as that of Fig. 4 was used: a rigid system of 30 filaments at $\pm 35°$, propelling a 15-pN load.

Because the energy required for polymerization is proportional to the distance protruded (Fig. 4 *a*), the distribution of potential polymerization energies mirrors the distribution of barbed-end distances from the load (Fig. 5 *a*). The large relative number at $\Delta E = 0$ account for filaments polymerizing from 1 δ or beyond, while the many potential events near $\Delta E = \Delta E_{\max}$ (8.1 kT) account for the contributions of the ever-present LE-supporting filament. (The distribution about 8.1 kT is due to the distribution of filament orientations about $\pm 35°$.) Of the overall energy distribution, only the subset shown polymerizes. These in turn perform work at the rate indicated, reflecting the shape of the work rate in Fig. 4 *b*. Note that the average work of protrusion (Eq. 4) for 30 filaments is only $8.1\ kT/30 = 0.27\ kT$, on the far lower end of the distribution. The system would exhibit maximum protrusion rate and effective stall force only if the work-sharing mechanisms in place resulted in all potential polymerization energies at this value. At the same time, this distribution is very different from that of a ZWS system, in which all events would require either $\Delta E = 0$ or $\Delta E = \Delta E_{\max}$.

Fig. 5 *b* shows the force-velocity relationship for this system, acquired by running a simulation with a slowly increasing load force f_L (proportional to F_L). The upper bound of any real or modeled system is indicated by PWS theory (Eq. 1), which decreases progressively from the free velocity. The ZWS lower bound (Eq. 2) is also indicated, but this relationship is only valid at low V_p/V_{free}. We therefore also ran a ZWS simulation with 30 filaments in which all barbed ends were initially positioned the same distance and 35° orientation from the load. The results began at V_{free} and decreased to match those of Eq. 2 with increasing load, as expected, and indicate the slowest possible average performance of a rigid, 30-filament system under Brownian motion. Comparatively, the velocity of the fractional WS case (with an initial distance distribution) is one-third to one-half of the way between ZWS and PWS at lower loads, but effectively stalls at a relatively low load force.

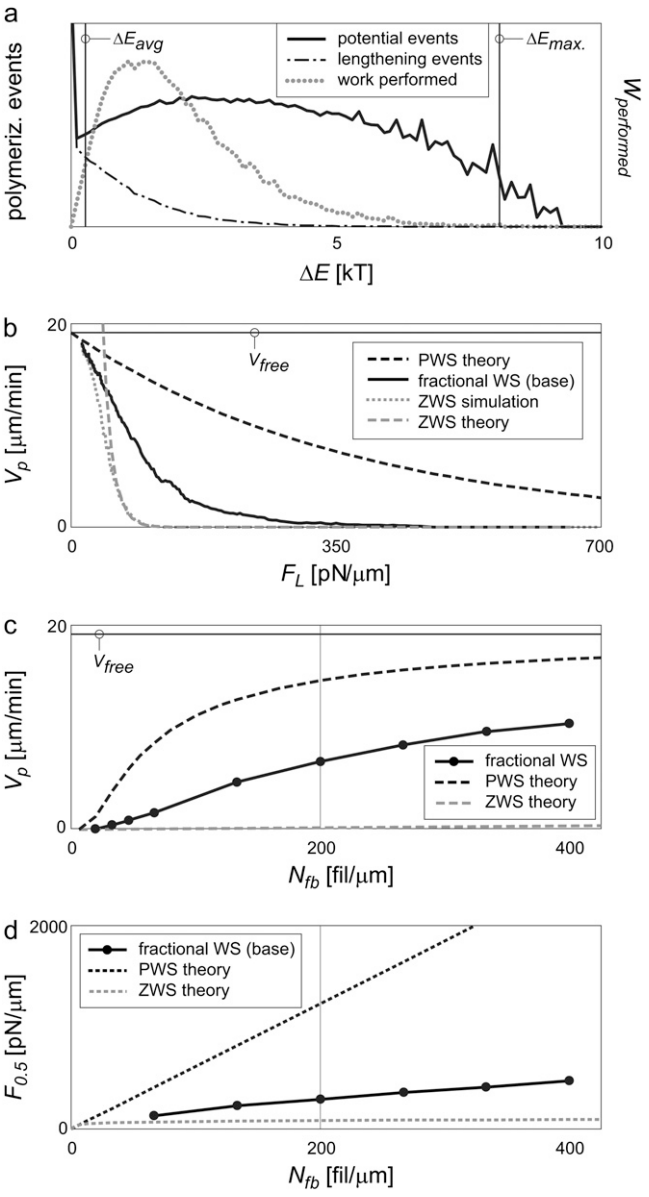

FIGURE 5 The fractional work-sharing allowed by the distance distribution is effective in increasing protrusion rates and stall forces. (*a*) The distribution of potential polymerization energies (work performed) is not limited to 0 and $\Delta E_{\max}$, but instead distributed broadly. (*b*) This results in a force-velocity relationship between ZWS and PWS performance limits. (*c*) While protrusion rates at internal membrane resistance levels (100 pN/μm) improve dramatically, (*d*) stall forces improve by relatively little compared to ZWS. A rigid LE under a 15-pN load was simulated, pushed by 30 rigid filaments. Other values are as in Table 2.

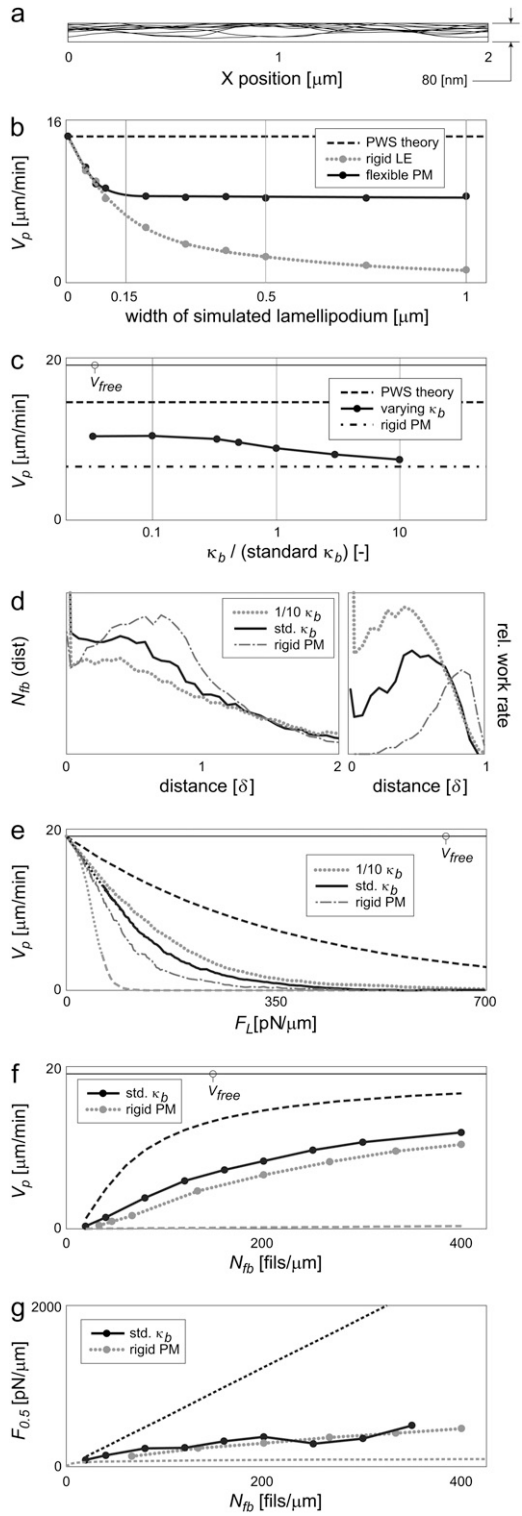

FIGURE 6 Membrane flexibility allows the effect of protrusion to remain local. (*a*) Allowing for membrane flexibility enables local shape fluctuations, although the overall shape remains optically straight even over long distances. Ten successive shapes shown at 12-s intervals, rigid filaments, no branch tethering. (*b*) With a rigid LE, increasing the width (i.e., load and number of filaments, proportionally) continuously decreases protrusion rate. A flexible LE limits the distance over which filaments can act, effectively limiting maximum load and preserving the performance of ≈150-nm sections to any width. (*c*) Compared to normal levels of membrane bending energy, decreasing κ_b (increasing flexibility) improves protrusion rates to a limited level. Physiologic $\kappa_b = 1 \times$ ''relative κ_b.'' (*d*) Fractional work-sharing is still in effect. (*e*) Force-velocity relationships and (*f*) protrusion rates at a given N_{fb} improve mildly over those of 150-nm-wide rigid systems, corresponding to the improvements shown in panel *b*. Wider rigid systems would decrease in V_p under any conditions, but membrane flexibility allows maintenance of the values shown at any width. (*g*) Stall forces remain low, however. Flexible membrane simulations specified 0.5-μm (wide) leading edges and rigid filaments. Other values are as in Table 2. Bounds for PWS and ZWS are as in Fig. 5.

The relationship between V_p and N_{fb} is shown in Fig. 5 *c*, plotted with PWS and ZWS bounds. Protrusion rates increased with N_{fb} relative to the PWS limit, indicating that the larger population has more opportunity to polymerize at low-energy events. Fig. 5 *d* shows the relationship between effective stall force ($F_{0.5}$) and N_{fb}. Unlike the ZWS system, the system with a distance distribution increases $F_{0.5}$ values significantly with N_{fb}, but still remains far less forceful than a PWS system. A system that allows for a variety of distances from filament to load therefore protrudes much faster than the worst possible system, with a more modest gain in force generation.

A flexible plasma membrane allows for consistent performance, independent of LE width

Membrane-bound organelles such as lamellipodia and filopodia enable thermal motion to create local gaps for protrusion, allowing for lower-energy polymerization events. Because curved membranes naturally create variations in distance between filaments and the membrane, we compared the improved performance of membrane-bound systems to those utilizing only a distance distribution. Filaments were maintained rigid throughout.

Ten successive LE profiles of a 2-μm-wide simulation varied up to 80 nm in the *Y*-direction, almost 30 times the monomer step size (Fig. 6 *a*). Note that 80 nm is still much less than the wavelength of light, such that these fluctuations would not be visible by common optical microscopy techniques. Because the variations occur over length scales much shorter than 2 μm, the LE is expected to remain optically straight over even larger widths. The flexible membrane therefore allows for some redistribution of loads among working filaments, but does not by itself lead to the widely variable lamellipodial morphology seen in vivo.

A PWS system would maintain the PWS V_p under any application of the same average force per filament (F_L/N_{fb}). In contrast, increasing the load force on a rigid LE, even with a proportional increase in the number of filaments (i.e., increasing LE width but maintaining F_L/N_{fb}), causes a continuous decrease in protrusion rate (Fig. 6 *b*). A flexible membrane system behaves in an intermediate way. Protrusion rate initially decreases with width, but then remains

constant at greater than ≈150 nm. This indicates the extent to which the flexible membrane allows filaments to act locally. Membrane displacements are not transmitted across very large distances, and in this sense filaments act only relatively locally and do not sense distant loads. A wide swath of lamellipodium, with its increased total load and filament count, consequently protrudes at the same rate as a 200-nm section. However, work-sharing over distances less than ≈100 nm is not aided by this flexibility, since the bending resistance of the lipid bilayer does not allow for small-radius curvature. Over these short distances, the flexible LE and rigid LE behave similarly (Fig. 6 *b*). A plot of $F_{0.5}$ as a function of lamellipodial width is qualitatively similar, with curves at PWS performance for one filament, diverging at ≈100 nm, and then either remaining constant or decreasing for flexible or rigid membranes, respectively (not shown). The flexible membrane thus allows filaments to share the work of lamellipodial protrusion by operating only relatively locally, though not so locally (independently) as to achieve PWS. Any flexibility in the actin network would allow the filaments to work independently over some distance even against a rigid load by letting the network conform to the load. Experiments in which a beam was used to indent the LE of moving keratocytes suggests that this distance is on the order of microns, much longer than that which a membrane can conform to Prass et al. (23). Such network flexibility would set a small lower limit on the diminishing V_p of the rigid LE in Fig. 6 *b*.

Fig. 6 *c* depicts the protrusion rate of 200 fil/μm against a wide, flexible LE of varying bending energy κ_b. Increasing κ_b from the physiologic value stiffens the LE, decreasing V_p appropriately toward the limit set by the rigid-LE simulation (of Fig. 5). Decreasing κ_b increases V_p, but still does not allow for perfect work-sharing.

There are typically 20 filaments acting over 100 nm of LE. Consistent with the absence of local work-sharing over these small regions, the characteristic distribution of filament distances from a wide LE is still evident (Fig. 6 *d*). While 11% of filaments support the membrane at any one time, the trailing 89%, peak in work rate at ≈0.6 δ from the LE. Furthermore, a polymerization event from the LE still requires 4.6 kT ($e^{-4.6} = 0.01$). Fractional work-sharing thus remains critical for the protrusion of a flexible membrane.

This local work-sharing improved performance only modestly over that of rigid, 150 nm-wide systems. Higher V_p values arose in force-velocity relationships, especially at intermediate loads (Fig. 6 *e*). Protrusion rates at the standard 100 pN/μm load were consistently higher (Fig. 6 *f*), though the effective stall force performance was not improved significantly (Fig. 6 *g*). Fig. 6 *b* showed that the discrepancy between a rigid and a flexible LE progressively increases with section width. Therefore, while the local work-sharing enabled by the flexible LE does not result in high V_p or $F_{0.5}$ performance of small systems, it enables the maintenance of those performance levels across all larger lamellipodial widths.

Filament flexibility can by itself enable perfect work-sharing protrusion velocity and effective stall force

Not only can rapidly-fluctuating flexible filaments allow for polymerization gaps (7), but they can also allow multiple nearby filaments to be simultaneously compressed under the load. This in turn allows nearby filaments to share the load force and protrusive work. However, because a load can bend a cantilever-like filament until it is parallel to the LE, where subsequent polymerization would be rapid and load-free, the cell must limit filament length. For a relatively high average load of 1 pN/filament, such a debilitating distortion occurs at bending lengths l_b of ≈240 nm. In the following simulations, a wide range of filament flexibilities over a $0 < l_b < 200$ nm range were allowed, as were the inevitable filament-load distance variations. For simplicity, all pushing filaments in a simulation were assumed to have the same constant bending length. The LE was held rigid and under a 15-pN load.

We first investigated the dependence of protrusion rate on bending length. Velocities at low bending-length matched those of rigid filaments, while high ones asymptotically approached the PWS rate (Fig. 7 *a*). Using our standard of 30 filaments pushing a 15-pN load, protrusion rates increased from 6.5 μm/min for rigid filaments to 13.7 μm/min for filaments of 150-nm bending length, 94% of the PWS rate. Higher-loads exhibited even larger relative increases over fractional work-sharing performance. The same number of flexible filaments pushing a 30-pN load increased in protrusion rate by 6.9-fold over rigid filaments, while the velocity of a 60-pN load increased by 38-fold, both again approaching PWS velocities near 150-nm bending lengths. Because filament flexibility is proportional to the third power of the bending length l_b, and V_p was limited to PWS performance, the curves exhibit a delayed upswing and sigmoidal shape.

We have previously referred to fractional work-sharing in the sense that some filaments simply support the load until others protrude it. In this sense, moderate bending lengths may utilize this mode of work sharing, but very long lengths do not. Fig. 7 *b* compares the barbed-end distances of the rigid system with that of a system using fixed bending lengths. While one filament supported the LE in a rigid system, 27% of 40-nm filaments simultaneously supported the load and required only 1.8 kT to polymerize from the LE. Compared to the rigid filament peak work rate position of 0.8 δ, 40-nm filaments peaked at 0.25 δ behind the LE, and very flexible 100-nm filaments performed almost no work from behind the LE (Fig. 7 *c*).

The distribution of polymerization energies is consistent with fractional work-sharing for 40-nm but not 100-nm filaments (Fig. 7 *d*). Compared to the rigid system, 40-nm filaments have a ΔE distribution shifted toward zero but still quite broad, with 25% of potential events requiring >2 kT ($e^{-2} = 0.14$). Very flexible, 100-nm filaments began to approximate the PWS distribution, however, with the most

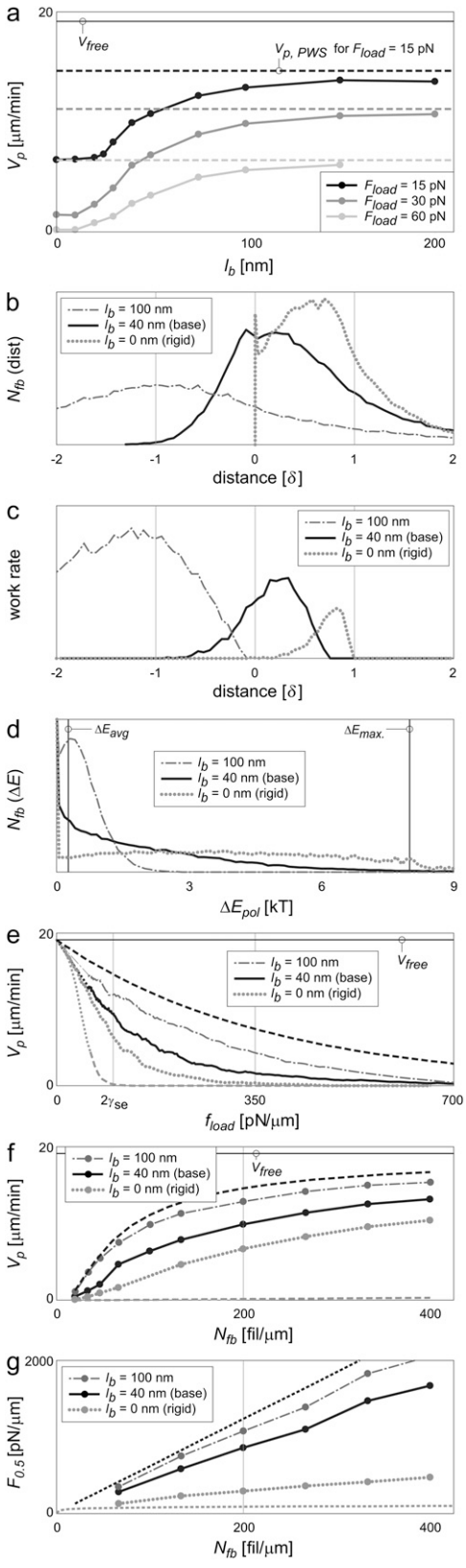

FIGURE 7 Filament flexibility can improve performance to near-ideal levels. (*a*) Protrusion rates increase with filament flexibility (proportional to l_b^3) to near-perfect levels at 150–200 nm, with relative improvements especially high under higher loads. (*b* and *c*) Fractional work-sharing is still in effect for moderately flexible filaments, but not for very flexible ones. (*d*) Very flexible filaments yield polymerization energy histograms that mimic those of PWS. (*e*) Filament flexibility shifts force-velocity relationships upward, improving both (*f*) protrusion rate and (*g*) stall force to levels near those of PWS. A rigid LE was simulated. Other values are as in Table 2. Bounds for PWS and ZWS are as in Fig. 5.

common energy required (besides zero) very near ΔE_{avg}. Filaments of moderate bending lengths, therefore, utilize a combination of fractional and simultaneous work-sharing mechanisms, while high filament flexibility precludes fractional work-sharing.

Systems with flexible filaments generally exhibited considerably higher velocities and effective stall forces. Force-velocity curves showed higher velocities at all significant loads (Fig. 7 *e*), and did not exhibit the irregular velocities often seen with rigid filaments at high loads. At N_{fb} values >50 fil/μm, filaments with 40-nm bending lengths protruded at rates of a consistent ≈ 3 μm/min faster than those relying only on fractional work-sharing (Fig. 7 *f*). Filaments of 100-nm length exhibited almost PWS velocities. Effective stall forces ($F_{0.5}$) for this system were increased dramatically over those of rigid systems or flexible membranes (Fig. 7 *g*), requiring 129 pN to effectively stall 30 filaments of 40-nm bending length (equivalent to $F_L = 860$ pN/μm). In summary, very flexible filaments can exhibit near-ideal performance. Flexible filaments of moderate (40-nm) length exhibit mildly improved velocities over systems with flexible membranes, but provide a far superior ability to generate significant protrusion in the face of high loads.

Under tethering forces, lamellipodial protrusion velocity can decrease with filament flexibility

We then considered the full lamellipodial model, with a flexible membrane, flexible filaments, and the dendritic nucleation (branching) model with self-organizing filament positions and orientations. Because branching was allowed, we incorporated the branch-tethering model as well, and first investigated the effects of tethering forces on performance. Tethering was not expected to alter effective stall forces, as protrusion distances are very small over the lifetime of a tether under near-stall conditions, and we therefore concentrated on its effect on protrusion rates.

Fig. 8 *a* demonstrates the effect of tethering on membrane protrusion, showing six successive LE shapes at 100-ms intervals for the full, tethered lamellipodium model. Tethering is evidenced by the local delay and release of the LE, affecting membrane shape and, thereby, nearby filament loads.

In an unexpected contrast to untethered systems, the protrusion rates of tethered filaments peaked and then decreased with longer bending lengths. Fig. 8 *b* plots the protrusion rates of the lamellipodial model as a function of filament bending length for various tethering assumptions. Without

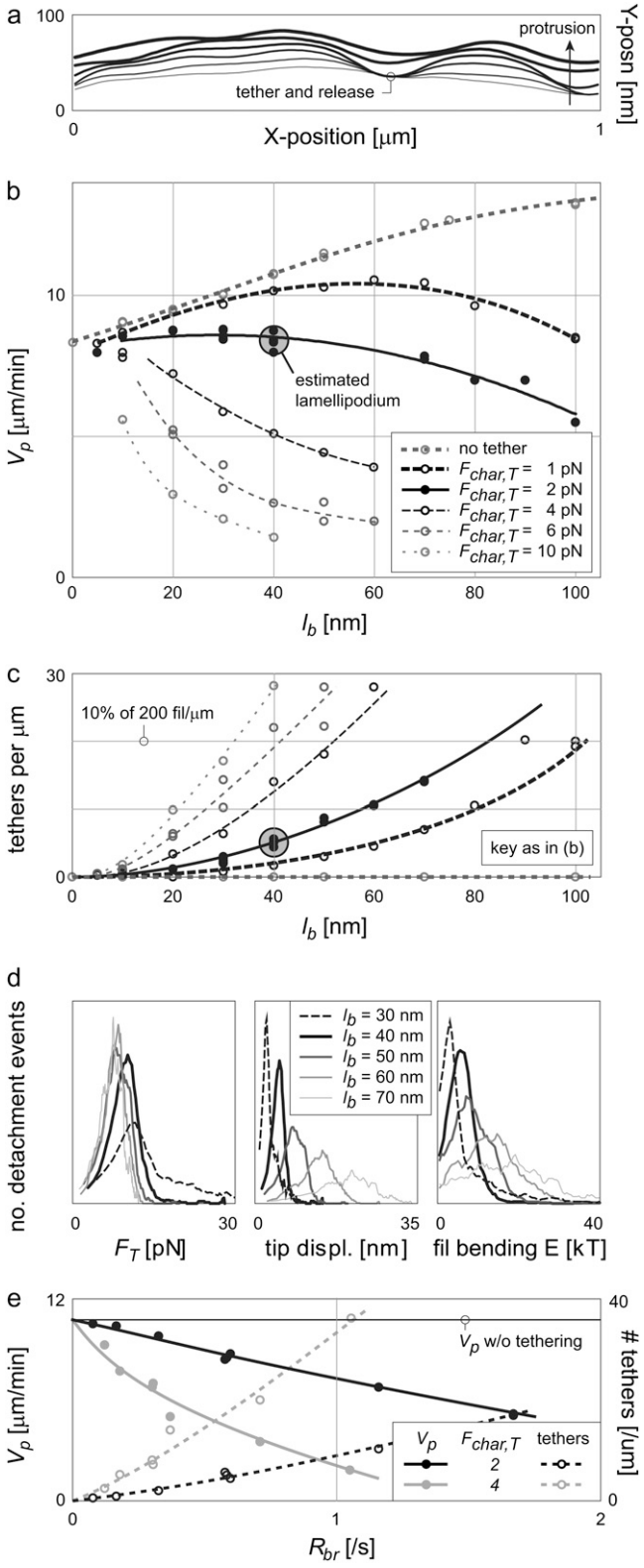

FIGURE 8 Transient branch-tethering limits the effectiveness of flexible filaments. (*a*) Fluctuations in LE shape exist due to transient delays in protrusion. (*b*) While the velocities of untethered lamellipodia increase with more flexible filaments, the protrusion rates decrease again with longer, tethered filaments. Increasing characteristic tethering forces ($F_{\mathrm{char,T}}$) magnifies this effect. (*c*) The number of tethered filaments increases with l_b and $F_{\mathrm{char,T}}$. (*d*) Tethered filaments tend to detach at similar forces regardless of filament flexibility (*left*), though more flexible filaments are displaced much farther to generate those forces (*middle*). The mechanics of cantilever beams stipulate that, given the same force, the increased displacement of the more flexible filaments contains more potential energy (*right*). This energy is accumulated via the work of pushing (i.e., untethered) filaments. (*e*) The net branch rate is the rate at which tethers are generated. Higher branch rates increase the instantaneous number of tethers and subsequently decrease protrusion rate, as shown. Other values are as in Table 2. Bounds for PWS and ZWS are as in Fig. 5. Large shaded circles indicate estimated lamellipodial operation.

tethering, protrusion rates increase continuously with bending length, consistent with expectations and Fig. 7 *a*. With a characteristic tethering force ($F_{\mathrm{char,T}}$) of 1 pN, however, protrusion rates peak near 60-nm lengths, while a $F_{\mathrm{char,T}}$ value of 2 pN protrudes fastest at bending lengths of <40 nm. Protrusion rates with $F_{\mathrm{char,T}}$ values of 4 pN or more peak at unphysiologically small bending lengths. Existence of this phenomenon is not dependent on a flexible LE; simulations run with tethering and a rigid LE exhibited similar V_p peaks (not shown).

The eventual decrease in V_p of Fig. 8 *b* is not due to an ultimate decrease in the level of work-sharing. There is a continuous increase in the number of filaments bent under the LE with increasing filament flexibility, leading to reduced loads and polymerization energies per filament (not shown). Fig. 8 *c* suggests a countering trend, however: the number of tethered barbed ends increases with both filament length and characteristic detachment force. A decreased tether dissociation rate is in fact expected with increased $F_{\mathrm{char,T}}$ values, because attachments are stronger, and with increasing l_b values because more flexible ''springs'' require larger displacements to generate the same forces.

The question remains as to why an increased number of more flexible tethers would necessarily slow protrusion, despite improved work-sharing. The slower protrusion is not due to a decrease in the number of polymerizing filaments, as V_p is a weak function of N_fb in this region (see Fig. 9 *d*, below). Fig. 8 *d* explains this instead as a natural consequence of the spring-like behavior of the filaments. Although detachment of tethers is dependent on both tether force and time, filaments over a wide range of flexibility reach similar tether forces before detaching (Fig. 8 *d*, *left*). To reach these forces, the tips of more flexible filaments are displaced farther before detaching (Fig. 8 *d*, *middle*). It is this increased displacement that explains the lower performance. At any given tether force F_T, the amount of potential energy accumulated in a linear spring (e.g., each filament cantilever beam) is proportional to the displacement of the tip,

$$E = \frac{1}{2}\left[\frac{3L_\mathrm{p}kT}{l_\mathrm{b}^3}\right]\chi_\mathrm{tip}^2 = \frac{1}{2}\kappa\chi_\mathrm{tip}^2 = \frac{1}{2}F_\mathrm{T}\chi_\mathrm{tip}, \qquad (3)$$

where κ is the spring stiffness constant, itself dependent on filament persistence length L_p and bending length l_b. The

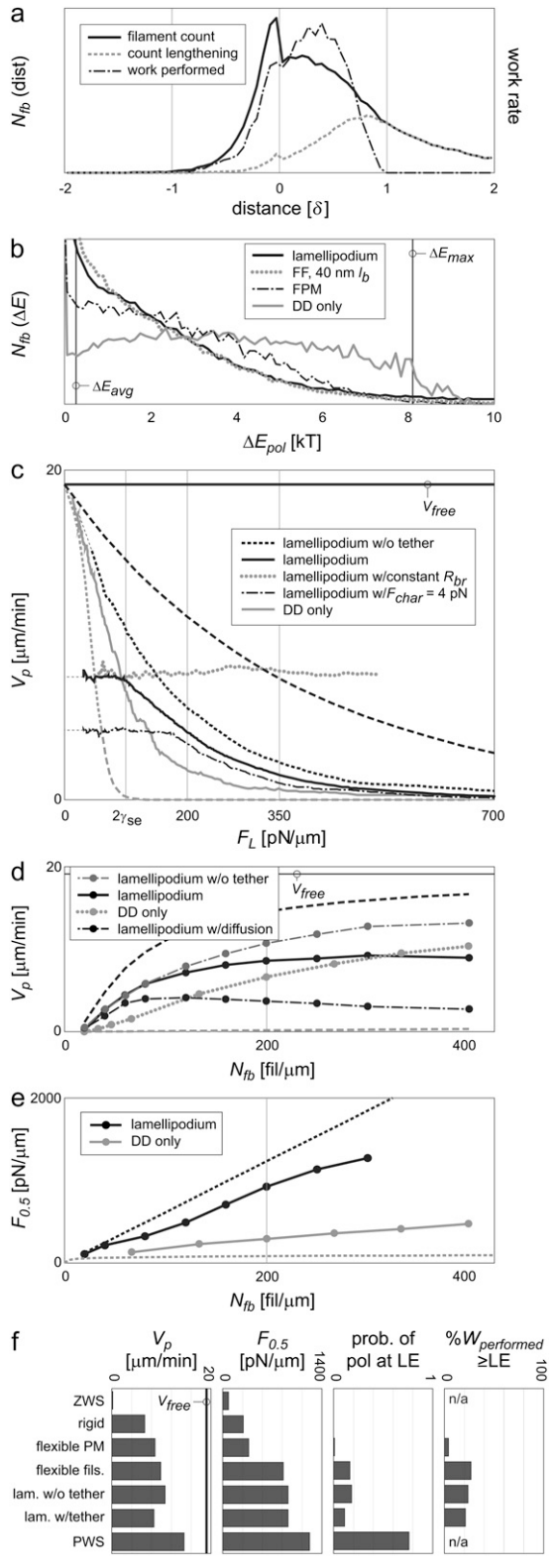

FIGURE 9 The full lamellipodial model with tethered branches uses all three modes of work-sharing but exhibits only moderate performance. (*a*) Fractional work-sharing remains an effective and important mechanism of distributing the work of protrusion. (*b*) The distribution of energies in modeled lamellipodia mimic those of moderately flexible filaments. (*c*) Tethering changes the shape of the force-velocity curve such that protrusion rate is insensitive to external load at low loads, and approaches untethered performance at high loads. Increasing $F_{\mathrm{char,T}}$ results in longer plateaus at lower velocities. All curves but one are shown for constant $N_{\mathrm{fb}} = 200$ fil/μm (varying R_{br}); a constant branch rate instead maintains a velocity independent of load. (*d*) Both tethering and diffusion counter the effect of increased filament counts, such that the protrusion rate is a very weak function of N_{fb} greater than ≈60 fil/μm. (*e*) Stall forces are similar to those of flexible filament simulations, deviating from PWS performance at low filament counts. Bounds for PWS and ZWS are as in Fig. 5. (*f*) Compared to other systems analyzed, tethered lamellipodia models exhibit moderate velocities and the gains in effective stall force of flexible filaments. The fraction of work performed by bent filaments is still low, demonstrating the importance of fractional work-sharing. Values are as in Table 2.

displacement of the filament tip (spring) in a direction perpendicular to its unbent length is χ_{tip}. Because the tethers detach at similar forces, this has the effect that filaments with higher bending lengths tend to have higher accumulated potential energies upon breaking (Fig. 8 *d*, *right*). The work done in bending these tethered filaments is ultimately performed by free, pushing filaments and therefore represents work diverted from protrusion. The peaks in Fig. 8 *b* are thus a balance of two competing effects: At low l_{b}, the improving efficacy of work-sharing dominates, while at higher l_{b} the diversion of energy to the bending of tethers dominates. An increase in the characteristic tether force $F_{\mathrm{char,T}}$ amplifies this effect and decreases the bending length of peak V_{p}.

Because one tether-and-release event accompanies each branch event, the branching rate affects the level of internal resistance and the protrusion rate. Increasing the value of ε from 1.5 δ to 2 δ increases the fraction of N_{fb} within the branch-inducing, cap-protective zone and so decreases the required R_{br} to maintain the same N_{fb}. Protrusion rates subsequently rise, but peak near a similar l_{b} (not shown). Fixing l_{b} at 40 nm but varying R_{br} over a wide range (and ε, to maintain an N_{fb} of 200 fil/μm) results in the values of Fig. 8 *e*. The number of tethers increases with branch rate as shown, consequently decreasing the protrusion rate. Based on the large velocity penalties of long l_{b} and high $F_{\mathrm{char,T}}$, as well as limits on the self-organizing behavior of filament orientation (24), we estimate that lamellipodia operate with ≈40-nm filament bending lengths, ε-values of 1.5 δ, and a characteristic tethering force $F_{\mathrm{char,T}}$ of 2 pN (Table 2).

Lamellipodia rely on all three mechanisms of work-sharing, but polymerization events still do not share the work of protrusion equally

With the full lamellipodial model and estimated operating parameters listed in Table 2, all three modes of work-sharing were important to performance. Peak work rates were performed from a position 0.4 δ behind the local LE, and only 21% of the total work was performed by filaments supporting the LE, indicating the importance of fractional work-sharing in this flexible system (Fig. 9 *a*). Protrusion rates of the LE were independent of LE width above small values, only

possible with a flexible membrane and the local work-sharing it enables. Finally, an average of 32% of flexible, growing filaments supported, and were bent under, the LE at any one time. The distributed load forces and decreased polymerization energies allowed by this simultaneous work-sharing are evident in the energy distribution comparisons of Fig. 9 *b*, where lamellipodial distributions mimic those of flexible filament systems. Compared to simulations with a flexible LE and rigid filaments, which required an average of 4.6 kT to polymerize from the LE, lamellipodia with untethered and tethered filaments only required 1.7 and 2.2 kT, respectively.

The shape of the force-velocity relationship was made quite different by tethering. While the untethered lamellipodial system followed the familiar general shape of the PWS limit, the tethered system had velocities essentially independent of total load force at low values. With the standard 2 pN $F_{\mathrm{char,T}}$ value, protrusion rates remained at $\approx$8 μm/min to (surface energy and external) loads of 100 pN/μm, while with 4 pN $F_{\mathrm{char,T}}$ values, protrusion rates were limited to $\approx$5 μm/min to loads of 180 pN/μm (Fig. 9 *c*). In these constant-velocity regions, polymerization rate appears limited not by external loads but largely by the tether detachment rate. There, characteristic tether forces are relatively high compared to load forces, and tethered filaments are progressively bent by rapidly-polymerizing working filaments until tethering ultimately stalls local protrusion. The detachment rate of the tether is the rate at which the LE is released to spring forward. As load forces increase, the polymerization rate of working filaments becomes slower and more limiting. At very high resistance forces, tethers are released before accumulating significant strain and therefore do not contribute to total resistance and do not slow protrusion. Protrusion rate is therefore somewhat constant at low load and approaches those of the nontethered system at high load. Note that, as before, these curves represent systems in which the branching rate was controlled to maintain 200 forward-facing filaments per micron (i.e., R_{br} was continuously adjusted with changing V_{p} such as to maintain 200 fil/μm). If the model were to instead exhibit constant-R_{br}, autocatalytic branching, N_{fb} would rise as needed to maintain a constant protrusion rate (Fig. 9 *c*) (3,24).

The ability of this system to share the work of protrusion among polymerization events is not nearly enough to approximate ideal velocity or effective stall force performance. The untethered system achieves 74% of V_{free}, but the tethered system only reaches 45% of the ideal rate (Fig. 9 *d*). As a function of filament density, the untethered and tethered velocities are the same at low densities because protrusion and branching rates are low. The curves diverge above 60 fil/μm. When the diffusion model is activated, maintaining a 12-μM soluble actin concentration 1 μm behind the LE, the monomer concentration at the LE decreases with the total rate of polymerization. This serves to flatten the curve and make the protrusion rate a very weak function of filament density above 60 fil/μm (Fig. 9 *d*). It is difficult to estimate the level of recycling of actin monomers toward the LE, as this depends on depolymerization and ATP-recycling rates. Using the cofilin-adjusted depolymerization rates and debranching rates noted in Table 2, however, extending the fixed-concentration to 3 μm from the LE makes little difference in performance (not shown). The effective stall force retains most of the advantage of the flexible filaments (Fig. 9 *e*), enabling protrusion up to a total load of 670 pN/μm, almost sevenfold the membrane resistance. The performance of lamellipodia in comparison to the other systems discussed is summarized in Fig. 9 *f*.

Given the computed level of work-sharing, the natural monomer size results in the maximum possible protrusion rate

The evolution of monomer size likely depended on a variety of factors, perhaps including filament rigidity, metabolic cost of assembly, diffusivity, and protrusion performance. Filament orientation can reduce the effective monomer size by changing the distance that a polymerization event will move the tip forward. Filament angles optimal for maximum protrusion rate have been calculated (7). That analysis assumed PWS and the resulting optimal orientation was the direction of protrusion until relatively high loads, suggesting that larger monomers might be beneficial. In light of the imperfect work-sharing shown here, we varied the monomer size itself in successive runs to measure its effect on protrusion rate and effective stall force under different conditions. Filament orientation was maintained at $\pm 35^\circ$ ($\theta_{\mathrm{br}} = 70^\circ$) with a standard deviation σ_{br} of 7°.

The effective stall force ($F_{0.5}$) is plotted in Fig. 10 *a* as a function of monomer size. Theory predicts that effective stall force will continuously rise to very small δ-values, displaying no optimum over the region shown (Eq. 7). At the natural monomer step size of 2.7 nm, the values shown match those of Fig. 9 *e*. As monomer size decreases, performance approaches that of PWS because the monomer size is a smaller fraction of the filament and LE bending displacements. A cell primarily concerned with generating high protrusion forces would likely have employed a smaller monomer size. Reducing the δ-value by 50% would result in a 93% increase in $F_{0.5}$ and a 22% decrease in V_{p}.

Regarding protrusion rate, there exists an optimal δ-value at which V_{p} is maximized. At very large δ, V_{p} is limited by the high work of polymerization and so monomers add at a very slow rate. At very small δ, monomers add at nearly the free rate but V_{p} is limited by the small step size. For the standard loads of 15 pN per 30 filaments (100 pN/μm and 200 fil/μm) analyzed in this article, this optimal δ-value in PWS (Eq. 1) is 10.0 nm, $\approx 4\times$ the natural value (Fig. 10 *b*). In contrast, a ZWS system requires a much smaller, 0.9-nm δ-value for maximum V_{p} (Fig. 10 *b*). (Note that this value is not that computed by the ZWS theory (Eq. 2), as the protrusion rates are high enough to make that prediction inaccurate; it is a

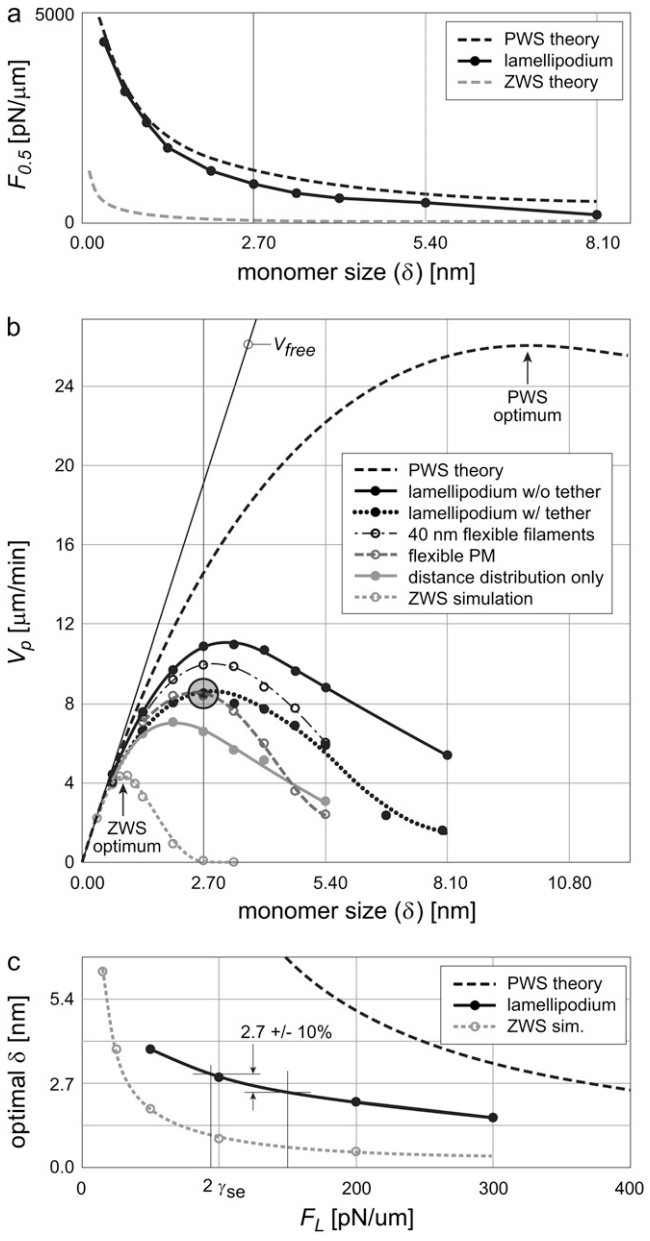

FIGURE 10 The moderate overall performance of tethered lamellipodia corresponds to the evolved monomer size. (*a*) The effective stall forces generated by lamellipodia increase continuously with decreasing monomer size, and remain relatively close to PWS values. (*b*) There is an optimal monomer size for velocity generation, however. Systems exhibiting ZWS protrude fastest with only a 0.9-nm monomer step size. Increasing system flexibility increases performance and optimal monomer size to near those found in vivo, and tethered lamellipodia ($\varepsilon = 1.5\ \delta$) exhibit peak protrusion rates near the natural $\delta = 2.7$ nm. In contrast, systems exhibiting PWS would protrude much faster at very large, 10-nm step sizes. Large shaded circle indicates estimated lamellipodial operation. (*c*) Shown as a function of total load force, the optimal step size for tethered lamellipodia is 2.7 nm ± 10% for membranes with ≈0–50 pN/μm external loads (90–150 pN/μm total loads). Other values are as in Table 2.

simulation result.) Between this wide optimal size range of 0.9 nm $\leq \delta \leq$ 10.0 nm, all systems with intermediate levels of work-sharing have optima. As work-sharing modes are added, first fractional, then local or simultaneous, and finally all three modes concurrently, the system is able to make optimal use of larger δ-values. The untethered lamellipodial model peaks in V_p at $\delta \approx 3.2$ nm, just larger than the natural δ-value. In the full lamellipodial model with transient tethering (and ε fixed at 1.5 $\delta = 4.05$ nm), velocities are reduced and the peak V_p is shifted to $\delta \approx 2.9$ nm (Fig. 10 *b*). We interpret this as suggestive that the level of work-sharing modeled herein is fairly accurate.

The set of curves relating V_p to δ in Fig. 10 *b* differ with load force. To examine this effect, Fig. 10 *c* plots only the optimal monomer size (for maximum V_p) as a function of load. The trends indicate that the optimal monomer size decreases with increasing load, as expected, with the natural value of $\delta = 2.7$ nm optimal for $F_L \approx 120$ pN/μm. The slope is fairly low for the standard tethered lamellipodium, however, and a value of 2.7 nm is within 10% of the optimal value for loads between 95 pN/μm and 150 pN/μm. We conclude that the full lamellipodial model, with tethering $F_{char,T} =$ 2 pN, $N_{fb} = 200$ fil/μm, and internal surface energy load forces of 100 pN/μm, operates under a level of work-sharing with which a monomer size of $\delta \approx 2.7$ nm exhibits a near-fastest rate of protrusion under 0 to ≈50 pN/μm external loads.

CONCLUSIONS

We have developed a two-dimensional model of protrusion, with stochastic simulation of filament kinetics for each individual filament, a flexible leading edge (LE) modeled after the plasma membrane, and flexible filaments modeled after cantilever beams. The model has a particular strength in that the energetics, and resulting probability, of each polymerization event are computed accurately and individually, such that lamellipodial protrusion by a population of filaments may be analyzed for the emergence of aggregate behavior and quantitative performance. Care was taken not to introduce ad hoc assumptions or values. We compared model performance to the theoretical limits of velocity and effective stall force generation, and showed that lamellipodia are unlikely to share the work of protrusion evenly among all working filaments.

Effective protrusion requires the generation of adequate velocity against resistive internal and external forces. The Brownian ratchet mechanism describes the concentration and rectification of thermal energy to this end by the polymerization of actin monomers, where the probability of an adequate polymerization gap existing decreases exponentially with the thermal energy required to create it (i.e., the protrusive work ultimately performed). Most models of actin protrusion make the assumption that each polymerization event performs the same amount of work on the load. This

assumed amount is indeed the average amount of protrusive work per polymerization event (Eq. 4), and incorporation of this assumption results in the protrusion rates and effective stall forces outlined in Eqs. 1 and 7. We have shown that these performance values are the best-case scenarios, or perfect work-sharing (PWS) performance. It is unlikely that a population of filaments operates in this manner, however. In the worst-case scenario, no event requires the average amount of energy, but instead requires either the maximal amount or zero. These zero work-sharing (ZWS) protrusion rates and effective stall forces are dramatically lower than those of PWS (Eqs. 2 and 9, Fig. 1). This envelope of possible performance is quite large for systems meeting any significant resistance, including lamellipodia. Where lamellipodia operate within these bounds has been unclear.

Protrusion performance is improved by at least three mechanisms which help distribute the work of protrusion among polymerization events. These mechanisms shift the distributions of work among filaments from the ZWS scenario toward the PWS scenario. The three putative mechanisms operate by reducing the effective size of a monomer (*fractional* work-sharing), allow protrusion to operate only relatively locally (*local* work-sharing), or distribute the force of protrusion among multiple filaments concurrently (*simultaneous* work-sharing). In general, these mechanisms can operate alone or in combination, and are not affected by the particular distribution of filament orientation angles. Zero work-sharing or fractional work-sharing alone approximates some experimental systems with rigid loads and parallel filaments (15). The addition of flexible filaments is analogous to rigid experimental systems with branched (angled, flexible) filaments, or bacterial/bead propulsion (13,16,21,22). Finally, filopodia operate with flexibility in the membrane but not in filaments (20), while lamellipodia and analogs have all three mechanisms available (23,25,26). A number of these and other published experiments have sought to measure the relationship between load force and protrusion velocity, utilizing a variety of experimental systems with different combinations of the three mechanisms. Results, both qualitative and quantitative, have varied widely, and their interpretation should be made in the context of their widely-varying capacity for work-sharing.

A distribution of distances from the barbed end to the load is difficult to avoid in any system, especially those with flexible filaments or a flexible LE. Even in the case of a relatively rigid system, variations in precise branching angle, curvature of the load (e.g., bead or pathogen surfaces), or simply nucleation at a variety of positions, will lead to varying distances. Our simulations of rigid systems show that distances randomly initialized will become organized under a load force, such that filaments are farther from the load than might be expected. More importantly, the work of protrusion peaks sharply at a distance most of one-monomer away. This phenomenon is unaffected by branching or filament orientation, and occurs over a wide variety of loads and velocities. A simulation in which rigid filaments are geometrically limited to integer numbers of monomers away from the load represents a ZWS system. For low protrusion rates, these simulations matched the ZWS theory closely (Eq. 2, Fig. 5 *b*), exhibiting only a fraction of the protrusion rate and effective stall force available with a distance distribution. Fractional work-sharing was an important component of every system tested except those with very flexible filaments.

Addition of a flexible LE allowed for local protrusion. Because a polymerization event still affected a membrane region spanning ≈150 nm, containing dozens of filaments, fractional work-sharing remained an important mode. Protrusion rates did increase mildly with membrane flexibility, but not to PWS rates. Overall, the flexible LE allowed for only moderate velocity and surprisingly low effective stall forces. Its effect on work-sharing, therefore, was not to raise the performance of small LE areas, but to allow for that consistent performance over leading edges of any larger width.

Very flexible filaments approached PWS performance in untethered systems, requiring near the average energy of polymerization for most events. They did not depend on fractional work-sharing, but operated with virtually all filaments in similar levels of compression against the LE. Moderate-length filaments of 40-nm bending length, however, did exhibit fractional work-sharing, with most filaments lagging behind the LE. These shorter lengths nevertheless displayed a large improvement in protrusion rate over that of rigid filaments, and a dramatically higher effective stall force. The generation of a high effective stall force in particular was a capacity of this simultaneous work-sharing not demonstrated by fractional or local work-sharing.

In contrast, flexible filaments which were transiently tethered to the membrane upon branching were, surprisingly, ineffective at high flexibility. Further investigation showed that increasing flexibility was accompanied by increased accumulation of potential energy in the bent tethered filaments, and that this represented work diverted from protrusion. Maximum protrusion velocity was possible at moderate bending lengths, a compromise allowing some simultaneous work-sharing but limiting wasted effort. To maintain reasonable performance, we estimate that lamellipodia with tethered branching typically operate with filaments of relatively short, 40-nm bending lengths and characteristic tether forces of only 2 pN. This is consistent with our previous conclusion that short filaments are required for ±35° orientation pattern formation (24). The low tether forces may be attained with increased VASP concentrations or other molecules that facilitate tether detachment.

Given these operating values (Table 2), lamellipodia utilize all three modes of work-sharing, including the universally important fractional work-sharing. Tethering reduces low-load speeds such that the force-velocity curve is sigmoidal and insensitive to external load at low total loads. Tethering also reduces the protrusion rate for a given number

of filaments, but does not affect the ultimate generation of force. In general, the model lamellipodium operates at an intermediate position between ZWS and PWS performance. With diffusion modeled, monomer depletion makes the velocity largely independent of the number of filaments. This, and the model result that variations in the LE shape are too small to image with light, suggests that the cell has other methods of protruding the LE locally. If the cell relies on filament count, it likely modulates the numbers less than ≈60 fil/μm.

We believe that the level of work-sharing modeled is accurate. Perfect and zero work-sharing conditions require monomer sizes of 10 nm and <1 nm for maximum velocity, respectively, but the model lamellipodium peaks near the 2.7-nm natural size. Under the level of work-sharing modeled, lamellipodia have monomer sizes optimal for the generation of velocity at 0 to ≈50 pN/μm external loads.

APPENDIX A: THE COMMONLY-ASSUMED PERFORMANCE OF A SYSTEM OF BROWNIAN RATCHETS REQUIRES THE PERFECT SHARING OF PROTRUSIVE WORK

While protrusion of the cell is ultimately driven by the free energy of actin polymerization, here we are not concerned with the polymerization reactions per se, but concentrate on the probability of sterically allowing the reaction to occur. That is, we are concerned with the probability of a local concentration of thermal energy large enough to create at least a monomer-size gap, within which polymerization is carried out at its usual free rate. This energy value is used in the Boltzmann factor to calculate the probability of that gap existing. Tethering between filaments and the LE is neglected in this treatment. See Table 1 for symbol definitions.

Regardless of the nature of resisting force, the average amount of thermal energy required per polymerization event is equal to the total rate of work performed on the object, $\dot{W}$, divided by the total rate of polymerization among all working filaments, $\dot{n}$:

$$\Delta E_{\text{avg}} = \frac{\dot{W}}{\dot{n}} = \frac{V_{\text{P}} F_{\text{L}}}{V_{\text{P}} N_{\text{fb}}/(\delta\cos\phi)} = \frac{F_{\text{L}}\delta\cos\phi}{N_{\text{fb}}}. \tag{4}$$

In the absence of clear experimental indication, the assumption that the Boltzmann factor restricts the on-rate only is commonly intuited and made. (By thermodynamic theory, it is only known that the Boltzmann factor is applied to the ratio of free $k_{\text{on}}/k_{\text{off}}$. If the effect increasing the off-rate is significant, the protrusion rate will be less sensitive to load than shown here.) Under this assumption, the rate of polymerization of an event requiring energy ΔE is $k_{\text{on}}[A]e^{-\Delta E/kT}$. This is true if fluctuations are more rapid than free polymerization, regardless of the geometry of the system and regardless of how or what component is bent to create the polymerization gap. The total rate of work performed by many polymerization events is the sum of the individual thermal energies required for polymerization. The average rate of protrusion ($\dot{W}/F_{\text{L}}$) for a steady-state distribution of polymerization (ΔE_{i}^{+}) and depolymerization (ΔE_{i}^{-}) energies is then essentially

$$V_{\text{P}} = \sum_{\text{i}=1}^{N_{\text{fb}}}\left[\frac{\Delta E_{\text{i}}^{+}}{F_{\text{L}}} k_{\text{on}}[A]\, e^{-\Delta E_{\text{i}}^{+}/kT} - \frac{\Delta E_{\text{i}}^{-}}{F_{\text{L}}} k_{\text{off}}\right]. \tag{5}$$

No assumptions concerning the particular distribution of energies among polymerization events are implicit in Eqs. 4 and 5. We can simplify Eq. 5 and arrive at a common relation for protrusion velocity against a load by assuming that each of the N_{fb} polymerization events per δ-step forward requires the same average energy $\Delta E_{\text{i}} = \Delta E_{\text{avg}}$ from Eq. 4:

$$V_{\text{P}} = \sum_{\text{i}=1}^{N_{\text{fb}}}\left[\frac{F_{\text{L}}\delta\cos\phi}{F_{\text{L}}N_{\text{fb}}} k_{\text{on}}[A]\, e^{\frac{-F_{\text{L}}\delta\cos\phi}{N_{\text{fb}}kT}} - \frac{F_{\text{L}}\delta\cos\phi}{F_{\text{L}}N_{\text{fb}}} k_{\text{off}}\right], \tag{6}$$

which reduces to Eq. 1.

To solve for the theoretical stall force, V_{p} is set to zero and F_{L} is solved for. This value, $F_0 = N_{\text{fb}}/(\delta\cos\phi)\ \ln(k_{\text{on}}[A]/k_{\text{off}})$, is independent of the extent of work-sharing. However, systems vary in the rate at which they approach this zero velocity condition with increasing load force (Fig. 1 *a*). Those that approach zero velocity very slowly make the stall force both difficult to measure in experiment and of little meaning. We therefore instead compare the force at which V_{p} is reduced to 0.5 μm/min (only ≈2.5% of the V_{free} = 19.1 μm/min for $[A] = 12$ μM and $\phi = 35°$):

$$F_{0.5} = \frac{-N_{\text{fb}}kT}{\delta\cos\phi}\ln\left[\frac{\frac{0.5\mu\text{m/min}}{\delta\cos\phi} + k_{\text{off}}}{k_{\text{on}}[A]}\right]. \tag{7}$$

These protrusion rates and effective stall forces may be optimized by the cell by altering protein size, shape, and kinetic activity, and by altering the number of pushing filaments N_{fb}. Equation 1 yields the fastest protrusion rates when $\Delta E_{\text{avg}} = kT$; very small monomers polymerize at the free rate but nevertheless protrude slowly, while very large monomers polymerize very slowly due to high energy requirements. Note that the effective (or ultimate) stall force has no optimal finite monomer size, but approaches infinity as the monomer size decreases to zero or ϕ nears 90°.

APPENDIX B: SYSTEMS OPERATING WITH PERFECT WORK-SHARING DISPLAY THE HIGHEST POSSIBLE VELOCITY AND FORCE-GENERATING PERFORMANCE

Eqs. 1 and 7 represent the protrusion rates and effective stall forces under the assumption that the total work of protrusion is divided perfectly evenly among all polymerization events (i.e., PWS). These represent the highest rates and forces theoretically attainable, with any distribution of polymerization energies (work) at about the average reducing effectiveness. To see this, note that all productive filaments are pushing the same LE at the same rate. There are two ways a distribution of polymerization energies could be attained. If certain filaments typically have higher polymerization energy requirements than others, those with higher requirements will not keep up with a LE moving at least as fast as that protruded by the average energy. They would be lost to capping. If instead there was a distribution of energy requirements across polymerization events of each filament, each filament would still polymerize at the ΔE_{avg} over the long term. The time between individual polymerization events of this filament is 1/rate, and thus the time to polymerize a given distance is the sum of the times for a series of N events. We compare this value (left-hand side) to the time to reach the same distance if all ΔE_{i} equal ΔE_{avg} (right-hand side):

$$\begin{aligned}
&\sum_{\text{i}=1}^{N}\frac{1}{e^{-\Delta E_{\text{i}}/kT}} \geq \sum_{\text{i}=1}^{N}\frac{1}{e^{-\Delta E_{\text{avg}}/kT}},\\
&e^{\Delta E_1} + e^{\Delta E_2} + \ldots + e^{\Delta E_N} \geq N\, e^{(\Delta E_1 + \Delta E_2 + \ldots + \Delta E_N)/N},\\
&\frac{e^{\Delta E_1} + e^{\Delta E_2} + \ldots + e^{\Delta E_N}}{N} \geq \left(e^{\Delta E_1}\cdot e^{\Delta E_2}\cdot \ldots \cdot e^{\Delta E_N}\right)^{\frac{1}{N}}.
\end{aligned} \tag{8}$$

The left side of Eq. 8 represents the arithmetic mean of the $e^{\Delta Ei}$ terms, while the right represents the geometric mean of the same series of terms. By the algebraic ''inequality of arithmetic and geometric means'' (27), the relationship in Eq. 8 is always true and thus a system with a distribution of

energies always progresses more slowly than a system consistently requiring ΔE_{avg}. No distribution can result in protrusion faster than that of Eq. 1.

APPENDIX C: ZERO WORK-SHARING YIELDS THE WORST SYSTEM PERFORMANCE

Because protrusion is driven by individual, uncoordinated polymerization events, each performing significant work, sharing of protrusive work is unlikely to be equal. The lowest performance the system can exhibit occurs when the distribution of work is most skewed. There, relatively few events perform the maximum work, while most others perform zero work. If all filaments are relatively rigid and share the same orientation and Y position, a rigid load rests on all ends simultaneously (Fig. 2 *a*). The next polymerization event will then be required to perform the maximum amount of work, $F_L\delta\cos\phi$. All other filaments will then quickly catch up, requiring zero thermal energy each. Any filament can be the lead filament, and so at low velocities ($N_{fb}\, e^{-FL\,\delta\cos\phi/kT} \ll 1$, much slower than the free rate) the velocity is the rate of lead-filament polymerization. This is proportional to the number of filaments and to the Boltzmann probability of having the very high $F_L\,\delta\cos\phi$ thermal energy concentrated in the system (see Eq. 2).

Equation 2 represents ZWS, and provides the lower bound of possible system velocities. Because the protrusion rate of this system decreases rapidly at only moderate load forces (Fig. 1 *a*), the load at which protrusion is slowed to near-zero, $F_{0.5}$, effectively indicates a stall force:

$$F_{0.5} = \frac{-kT}{\delta\cos\phi}\ln\left[\frac{\left(\frac{0.5\mu m/min}{\delta\cos\phi} + k_{off}\right)}{k_{on}[A]}\frac{1}{N_{fb}}\right]. \qquad (9)$$

The PWS and ZWS velocity and effective stall force relationships are plotted in Fig. 1, and show a wide range of possibilities. Intermediate levels of work-sharing result in intermediate velocities and effective stall forces. Equation 5 can be used to calculate V_p and $F_{0.5}$ analytically for small numbers of filaments.

We thank Edwin W. Taylor, Shin-ichiro Kojima, and Yvonne S. Aratyn for their support, extensive discussion, and reading of the manuscript.

We acknowledge funding from the National Institutes of Health grant No. GM 62431 (to G.G.B.) and the Northwestern University Feinberg School of Medicine Division of Pulmonary and Critical Care (T32 Grant) and Department of Cell and Molecular Biology (to T.E.S.).

REFERENCES

1. Pollard, T. D., and G. G. Borisy. 2003. Cellular motility driven by assembly and disassembly of actin filaments. *Cell*. 112:453–465.
2. Goldberg, M. B., and J. A. Theriot. 1995. *Shigella flexneri* surface protein IcsA is sufficient to direct actin-based motility. *Proc. Natl. Acad. Sci. USA*. 92:6572–6576.
3. Carlsson, A. E. 2001. Growth of branched actin networks against obstacles. *Biophys. J*. 81:1907–1923.
4. Carlsson, A. E. 2003. Growth velocities of branched actin networks. *Biophys. J*. 84:2907–2918.
5. Dickinson, R. B., and D. L. Purich. 2002. Clamped-filament elongation model for actin-based motors. *Biophys. J*. 82:605–617.
6. Gerbal, F., P. Chaikin, Y. Rabin, and J. Prost. 2000. An elastic analysis of *Listeria monocytogenes* propulsion. *Biophys. J*. 79:2259–2275.
7. Mogilner, A., and G. Oster. 1996. Cell motility driven by actin polymerization. *Biophys. J*. 71:3030–3045.
8. Mogilner, A., and G. Oster. 2003. Force generation by actin polymerization II: the elastic ratchet and tethered filaments. *Biophys. J*. 84: 1591–1605.
9. Peskin, C. S., G. M. Odell, and G. F. Oster. 1993. Cellular motions and thermal fluctuations: the Brownian ratchet. *Biophys. J*. 65:316–324.
10. Hill, T. L., and M. W. Kirschner. 1982. Bioenergetics and kinetics of microtubule and actin filament assembly-disassembly. *Int. Rev. Cytol*. 78:1–125.
11. Theriot, J. A. 2000. The polymerization motor. *Traffic*. 1:19–28.
12. Miyata, H., and H. Hotani. 1992. Morphological changes in liposomes caused by polymerization of encapsulated actin and spontaneous formation of actin bundles. *Proc. Natl. Acad. Sci. USA*. 89:11547–11551.
13. Cameron, L. A., M. J. Footer, A. van Oudenaarden, and J. A. Theriot. 1999. Motility of ActA protein-coated microspheres driven by actin polymerization. *Proc. Natl. Acad. Sci. USA*. 96:4908–4913.
14. Loisel, T. P., R. Boujemaa, D. Pantaloni, and M. F. Carlier. 1999. Reconstitution of actin-based motility of *Listeria* and *Shigella* using pure proteins. *Nature*. 401:613–616.
15. Footer, M. J., J. W. Kerssemakers, J. A. Theriot, and M. Dogterom. 2007. Direct measurement of force generation by actin filament polymerization using an optical trap. *Proc. Natl. Acad. Sci. USA*. 104:2181–2186.
16. Parekh, S. H., O. Chaudhuri, J. A. Theriot, and D. A. Fletcher. 2005. Loading history determines the velocity of actin-network growth. *Nat. Cell Biol*. 7:1219–1223.
17. Wiesner, S., E. Helfer, D. Didry, G. Ducouret, F. Lafuma, M. F. Carlier, and D. Pantaloni. 2003. A biomimetic motility assay provides insight into the mechanism of actin-based motility. *J. Cell Biol*. 160: 387–398.
18. Dogterom, M., and B. Yurke. 1997. Measurement of the force-velocity relation for growing microtubules. *Science*. 278:856–860.
19. Alberts, J. B., and G. M. Odell. 2004. In silico reconstitution of *Listeria* propulsion exhibits nano-saltation. *PLoS Biol*. 2:e412.
20. Atilgan, E., D. Wirtz, and S. X. Sun. 2006. Mechanics and dynamics of actin-driven thin membrane protrusions. *Biophys. J*. 90:65–76.
21. Marcy, Y., J. Prost, M. F. Carlier, and C. Sykes. 2004. Forces generated during actin-based propulsion: a direct measurement by micromanipulation. *Proc. Natl. Acad. Sci. USA*. 101:5992–5997.
22. McGrath, J. L., N. J. Eungdamrong, C. I. Fisher, F. Peng, L. Mahadevan, T. J. Mitchison, and S. C. Kuo. 2003. The force-velocity relationship for the actin-based motility of *Listeria monocytogenes*. *Curr. Biol*. 13:329–332.
23. Prass, M., K. Jacobson, A. Mogilner, and M. Radmacher. 2006. Direct measurement of the lamellipodial protrusive force in a migrating cell. *J. Cell Biol*. 174:767–772.
24. Schaus, T. E., E. W. Taylor, and G. G. Borisy. 2007. Self-organization of actin filament orientation in the dendritic-nucleation/array-treadmilling model. *Proc. Natl. Acad. Sci. USA*. 104:7086–7091.
25. Boukellal, H., O. Campas, J. F. Joanny, J. Prost, and C. Sykes. 2004. Soft *Listeria*: actin-based propulsion of liquid drops. *Phys. Rev*. 69: 061906.
26. Giardini, P. A., D. A. Fletcher, and J. A. Theriot. 2003. Compression forces generated by actin comet tails on lipid vesicles. *Proc. Natl. Acad. Sci. USA*. 100:6493–6498.
27. Garling, D. J. H. 2007. Inequalities: A Journey into Linear Analysis. Cambridge University Press. 19.
28. McGrath, J. L., Y. Tardy, C. F. Dewey, Jr., J. J. Meister, and J. H. Hartwig. 1998. Simultaneous measurements of actin filament turnover, filament fraction, and monomer diffusion in endothelial cells. *Biophys. J*. 75:2070–2078.
29. Abraham, V. C., V. Krishnamurthi, D. L. Taylor, and F. Lanni. 1999. The actin-based nanomachine at the leading edge of migrating cells. *Biophys. J*. 77:1721–1732.
30. Boal, D. 2002. Mechanics of the Cell. Cambridge University Press, Cambridge, UK.
31. Isambert, H., P. Venier, A. C. Maggs, A. Fattoum, R. Kassab, D. Pantaloni, and M. F. Carlier. 1995. Flexibility of actin filaments derived

from thermal fluctuations. Effect of bound nucleotide, phalloidin, and muscle regulatory proteins. *J. Biol. Chem.* 270:11437–11444.

32. Pollard, T. D. 1986. Rate constants for the reactions of ATP- and ADP-actin with the ends of actin filaments. *J. Cell Biol.* 103:2747–2754.
33. Pollard, T. D., and J. A. Cooper. 1984. Quantitative analysis of the effect of *Acanthamoeba* profilin on actin filament nucleation and elongation. *Biochemistry.* 23:6631–6641.
34. Carlier, M. F., V. Laurent, J. Santolini, R. Melki, D. Didry, G. X. Xia, Y. Hong, N. H. Chua, and D. Pantaloni. 1997. Actin depolymerizing factor (ADF/cofilin) enhances the rate of filament turnover: implication in actin-based motility. *J. Cell Biol.* 136:1307–1322.
35. Blanchoin, L., T. D. Pollard, and R. D. Mullins. 2000. Interactions of ADF/cofilin, Arp2/3 complex, capping protein and profilin in remodeling of branched actin filament networks. *Curr. Biol.* 10:1273–1282.
36. Schafer, D. A., P. B. Jennings, and J. A. Cooper. 1996. Dynamics of capping protein and actin assembly in vitro: uncapping barbed ends by polyphosphoinositides. *J. Cell Biol.* 135:169–179.
37. Mejillano, M. R., S. Kojima, D. A. Applewhite, F. B. Gertler, T. M. Svitkina, and G. G. Borisy. 2004. Lamellipodial versus filopodial mode of the actin nanomachinery: pivotal role of the filament barbed end. *Cell.* 118:363–373.
38. Mullins, R. D., J. A. Heuser, and T. D. Pollard. 1998. The interaction of Arp2/3 complex with actin: nucleation, high affinity pointed end capping, and formation of branching networks of filaments. *Proc. Natl. Acad. Sci. USA.* 95:6181–6186.